

A Stable Lithium-ion Battery SOH Estimation Framework for Suppressing Measurement Noise with Unknown Distribution

Wentao Ma, *Member, IEEE*, Jingsong Xue, Yang Li, *Senior Member, IEEE*, Peng Guo, Xinghua Liu, *Senior Member, IEEE*, Zhongbao Wei, *Senior Member, IEEE*, Yiwen Wang, *Senior Member, IEEE*, and Badong Chen, *Senior Member, IEEE*

Abstract—Existing methods for estimating the state of health (SOH) of lithium-ion battery (LIB) typically rely on the assumption that the distribution of noise (or outliers) in the measurement data is known. However, this assumption rarely holds true for LIB operating under real-word conditions. This article proposes a stable framework for accurate SOH estimation that accommodates noises with unknown distribution in both measurement data and label values. The framework combines generalized correntropy loss (GCL) with Savitzky-Golay (SG) filter and extreme learning machine (ELM) to obtain measurement data filter named SG-GCL and SOH estimator named generalized ELM (GELM), respectively. The SG-GCL filtering of the measurement data keeps the root mean square error (RMSE) within 0.0365%, and Pearson correlation between extracted feature and SOH improves by 0.4963, which in turn leads to the reduction of the RMSE metrics of the ELM for the estimation of the SOH by 43.69%. From the filtering results, feature extraction and estimation results proved its necessity and effectiveness. GELM effectively suppresses the influence of label value noise on the model in the training process, which reduces the SOH estimation RMSE index by more than 0.66%. The results from experiments with different distributional noise conditions show that the proposed SOH estimation framework has excellent and stable performance.

Index Terms—State of health, Savitzky-Golay filter, generalized correntropy loss, extreme learning machine, measurement noise with unknown distribution

This work was supported in part by the National Natural Science Foundation of China under Grant 62473308, the National Key R.D Program of China under Grant 2021YFB2401900, the Joint Fund project of the National Natural Science Foundation of China under Grant U21A20485, and the Science and Technology Plan Project of Xi'an under Grant 23GFW0071. Corresponding author: Wentao Ma, and Yang Li.

Wentao Ma, Jingsong Xue, Peng Guo, and Xinghua Liu are with the school of electrical engineering, Xi'an University of Technology, 710048 China (e-mail: mawt@xaut.edu.cn, 2221920068@stu.xaut.edu.cn, 2211921110@stu.xaut.edu.cn, liuxh@xaut.edu.cn).

Yang Li is with the Department of Electrical Engineering, Chalmers University of Technology, 41296 Gothenburg, Sweden (e-mail: yangli@ieee.org).

Zhongbao Wei is with the National Engineering Laboratory for Electric Vehicles, School of Mechanical Engineering, Beijing Institute of Technology, Beijing 100081, China (e-mail: weizb@bit.edu.cn).

Yiwen Wang is with the Department of Electronic and Computer Engineering, Hong Kong University of Science and Technology, Hong Kong (e-mail: eewangyw@ust.hk).

Badong Chen is with the Institute of artificial intelligence and robotics, Xi'an Jiaotong University, Xi'an, 710048 China (e-mail: chenbd@mail.xjtu.edu.cn).

Color versions of one or more of the figures in this article are available online at <http://ieeexplore.ieee.org>.

I. INTRODUCTION

Due to high energy density and long cycle life, lithium-ion battery (LIB) is widely used as power sources for electric vehicles [1]. However, as LIB is cycled, irreversible aging occurs within them, reflected in the degradation of maximum usable capacity and an increase in internal resistance. This can lead to reduced battery life and increased safety risks. In order to ensure the safe and reliable operation of LIB, the battery management system (BMS) has been developed [2]. The state of health (SOH) as one of the key parameters of BMS cannot be measured directly and must be estimated via measurement data [3]. However, the measurement data are susceptible to noise interference in complex environments, and thus how to perform accurately online SOH estimate using noisy measurement data remains a challenge [4].

At present, the mainstream methods for estimating SOH can be broadly categorized into two types: model-driven (MD) methods and data-driven (DD) methods [5-6]. MD methods require accurate equivalent circuit or electrochemical models and have the shortcomings of high complexity and inability to migrate between different batteries [7]. The DD methods, by contrast, only need to train a black-box model with the collected data and do not require priori knowledge of LIB [8]. The two key parts of DD methods for accurate SOH estimation are health feature (HF) extraction and model training [9]. SOH is the ratio of the LIB's current maximum capacity to its rated capacity and HF is data sequences containing LIB aging information [9].

Extracting HFs that accurately reflect battery aging is an important prerequisite for accurate SOH estimation using a DD method [10]. Charging of LIB almost always include both constant current (CC) and constant voltage (CV) modes, and many HFs can be extracted from the CC-CV charging process. Cai *et al.* [11] extracted two temporal HFs of high correlation with SOH from the CC and CV charging stages of LIB to achieve accurate SOH estimation. Zhou *et al.* [12] extracted two types of HFs, the relative rate of change of ohmic internal resistance and the peak of incremental capacity (IC) curve, from the collected discharge data and charging data, respectively. Then the correspondence between different aging stages and SOH was established by combining the two kinds of HFs. Considering the different charging habits, the complete charging curves may be difficult to obtain. Therefore, multiple HFs of short stages based on the upper and

lower bounds of the battery state of charge were extracted in [13]. Deng *et al.* [14] split the voltage-capacity curve of a battery during CC charging into multiple voltage intervals, each representing a SOH-related HF. However, due to the complexity of the operating environment of LIB, the above references do not take into account that the data may contain noise. He *et al.* [15] employed a moving average (MA) filtering method for the IC curves, and the Gaussian filter was used to smoothen the IC curve in [16]. In addition, a complete ensemble empirical mode decomposition with adaptive noise (CEEMDAN) approach was applied in [17] to decompose and denoise the feature data collected from the voltage profile. Meanwhile, Zhao *et al.* [18] utilized a Kalman filter to smoothen the temperature difference curve derived from the charging data, ultimately yielding a more refined HF temperature difference curve that is easier to extract. Recently, Xu *et al.* [19] and Li *et al.* [20] used SG filters for filtering the IC curve obtained through their respective methods. Zhang *et al.* [21] utilized Savitzky-Golay (SG) filters to process the voltage-temperature curves and the computed differential thermo voltammetry curves to suppress the noise on the curves. Multiple HFs extracted from voltage and temperature curves were filtered using SG algorithm in [22]. Among the aforementioned filters, the SG filter can provide improved performance in terms of computational complexity and noise suppression ability [23].

However, the filtering algorithm is not applied to the direct measurement data such as current and voltage in most previous studies. Instead, these measurement data are usually utilized to generate other signals before being sent to the filter. This can give rise to a concern that when the raw measurement data contain unknown distribution noise (or outliers), pre-processing these data can generate invalid data sequences that do not contain any physical information. This concern can invalidate the filtering objects of existing studies. Therefore to the best of this study, an unresolved question is raised for the first time and verified in a follow-up to the article: How can measurement data containing unknown distribution noise be processed directly and efficiently to ensure that the extracted HFs contain sufficient aging information?

Another key to the DD methods is model training. She *et al.* [24] introduced an integrated learning approach that initially trains multiple radial basis function neural networks (RBFNNs) and subsequently determines the weights of each RBFNN using random forests (RF), which can achieve precise SOH estimation. In Ref [25], an advanced two-stage attention-based long short-term memory (LSTM) neural network was introduced by fusing the encoder and decoder parts of the network with two distinct attention mechanisms, thereby optimizing the impact on both input and output, respectively. Wang *et al.* [26] used a hybrid neural network combining convolutional neural network and fully connected neural network to fully exploit the relationship between different HFs and battery capacity. Zhou *et al.* [27] designed a recursive Gaussian process regression (GPR) model with a one-step delayed feedback loop to merge the estimated SOH value at the previous moment with the HF at present. However, overly

complex estimation models are not practically applicable in BMS. By parameter identification of the HF extracted from the electrochemical impedance spectrum, Pang *et al.* [28] achieved accurate SOH estimation using a fitted quadratic function. Fu *et al.* [29] implemented the estimation of SOH based on an extreme learning machine (ELM) incorporating regularization in conjunction with the proposed improved electrochemical impedance spectral computation with fast Fourier Transform. A ridge regression model incorporating a regularization term was applied in [30].

Although the existing studies have achieved good estimation results, they have not considered the problem that the labeled values of the training data may contain outliers. For the source of outliers in labeled values, it contains two aspects. On the one hand, the labeled values used nowadays are all calculated by the ampere-hour integration method, which can cause cumulative errors. On the other hand, incomplete charging and discharging can result in calculated label values that do not accurately reflect the actual capacity. In response to the problem of labeled values containing outliers, almost all of the existing research has dealt with removing the data of cycles in which outliers are located. However, not using these data can lead to underutilization of the data already available. The scarcity of battery aging data presents a challenge, as utilizing limited datasets may compromise the estimation accuracy of the existing models. Therefore, this brings up another question: How to train a stable model when the labeled values of the training data contain outliers?

In order to solve the above two problems, this article proposes a framework that combines a stable filtering method and a stable training model for raw data. Firstly, the SG filter is chosen due to its lower complexity and stronger de-noising ability. The collected current and voltage curves are filtered and denoised using this method. Then, multiple short-time HFs are extracted from the curves obtained by filtering. The HFs having high correlation with SOH are selected under each dataset for the subsequent state estimation. Finally, the ELM as an easy-to-implement and effective neural network model is applied for SOH estimation. Moreover, both problems target unknown noise. In information theoretical learning methodology, the generalized correntropy loss (GCL) is proposed in [31] due to its stability and flexibility for unknown noise. Specifically, there is a generalized Gaussian kernel with adjustable parameters in GCL. In the generalized Gaussian kernel, the metric resembles l_2 -norm when the data are close in distance. As the distance between data increases, the metric resembles l_1 -norm and finally resembles l_0 -norm. It is through the geometric property that GCL achieves stability to noise (or outliers) as compared to least squares (LS) computation of l_2 -norm between data. Therefore, the GCL is chosen to resist the unknown noise interference in data in this work that a novel SG filter with GCL (SG-GCL) is further developed to enhance the quality of the input measurement data, and an ELM with GCL (called generalized ELM, GELM) is introduced to mitigate the impact of outliers in the label values of training data. The main contributions of this

article can be summarized as follows:

- 1) A stable filter called SG-GCL is proposed for the problem that the original measurement data contains unknown noise. The replacement of the error criterion in the traditional SG using the GCL makes the SG-GCL not only retain the properties of SG filtering, but also greatly improve its stability in the face of non-Gaussian noise. This provides a much better guarantee for the subsequent extraction of HF.
- 2) Pioneering a new perspective, the retention of outliers in label values during model training is explored. In response, the GELM based stable estimator is introduced to mitigate the influence of outliers during the training of labeled values. This ensures the accuracy of model estimation based on enhanced data utilization.
- 3) The proposed framework is validated on two datasets. The unknown distribution noise in the measurement data is effectively filtered out. The filtering of the unknown distribution noise in the measured data results in an improvement of 0.4963 in the Pearson correlation between the extracted HF and SOH, which in turn leads to a 43.69% decrease in the RMSE index of the ELM estimation of SOH. And the influence of SOH label outliers during model training is also well suppressed, which is reflected in the reduction of estimated RMSE for GELM by 0.66% compared to ELM.

The rest of the article is organized as follows. In Section II, the framework for SOH estimation is provided and the improved methodology used is derived. The dataset used in the article is elaborated in Section III. Section IV conducts filtering of measurement data and extraction of HF. In Section V, SOH estimation based on extracted HF is performed and compared from different angles. Section VI discusses the existing deficiencies in the work and future research directions. Finally, the article is concluded in Section VII.

II. METHODOLOGY

In this section, the proposed stable model used in each of the two stages of SOH estimation is derived in detail. The general framework of the SOH estimation method is shown in Fig. 1. It mainly consists of two parts: offline training and online estimation. Both offline training and online estimation involve measurement data contaminated with noise. The unknown distribution noise contained in each measurement data sequence is suppressed using the SG-GCL filtering method. And the labeled data containing noise only appears in the offline training part, and it only affects the training of the model. For this part of the noise the GELM model is used for suppression. The experiment on processing measurement data with noise will be presented in Section IV, and the experiment on processing label data with noise will be presented in Section V.

A. Generalized Correntropy Loss

Correntropy as a measure of local similarity is very

effective for non-Gaussian measurement noise with large outliers [32]. It has been used in several fields such as navigation systems [33], image classification [34], and state estimation [35]. Generalized correntropy, as a generalized form of correntropy, replaces the Gaussian kernel in the correntropy with a generalized Gaussian density function to achieve higher flexibility [31]. In the case of a finite number of samples $\{(x_i, y_i)\}_{i=1}^N$, the GCL can be defined as [31]

$$J_{GCL}(X, Y) = 1 - \frac{1}{N} \sum_{i=1}^N G_{\alpha, \sigma}(x_i, y_i) \quad (1)$$

$$G_{\alpha, \sigma}(x_i, y_i) = \exp\left(-\left|\frac{x_i - y_i}{\sigma}\right|^\alpha\right) \quad (2)$$

where $\alpha > 0$ denotes the shape parameter and $\sigma > 0$ is the scale parameter.

From (1) and (2), it can be analyzed that the GCL can limit the loss value to $[0, 1]$ regardless of the value of the adjustable parameter, which reduces the effect of large errors caused by outliers on the loss value. In contrast, LS based on l_2 -norm shows a regularity of power growth in the loss value as the error increases, which makes the local outliers in the data have a great impact on the loss function and leads to a negative impact on the overall effect of the algorithm. The comparison of the two losses is also displayed in Fig. 2. From Fig. 2, it can be seen that by tuning the different parameters, the GCL exhibits a more flexible and versatile localization property compared to the LS. Therefore, by adjusting the appropriate shape parameters and size parameters, the GCL can be made to adapt to different types of algorithms.

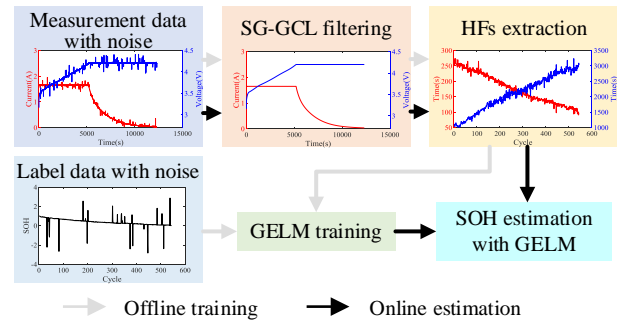


Fig. 1. SOH estimation framework.

B. Savitzky-Golay Filter with GCL

The SG filter [23] is based on the LS method of fitting a polynomial to the data within the window. As such, it has two main parameters namely window length and polynomial order. Considering a symmetric window of length $2m+1$ in a sequence of data $C = [c_{-m}, c_{-m+1}, \dots, c_0, \dots, c_m]$ and then a polynomial of order n can be utilized to fit it by minimizing the LS loss defined as

$$J_{SG-LS} = \sum_{l=-m}^m (\hat{c}_l - c_l)^2 = \sum_{l=-m}^m \left(\sum_{k=0}^n a_k l^k - c_l \right)^2 \quad (3)$$

where \hat{c}_l represents the l -th fitted value in the present window

and a_k denotes the coefficients of order k in the polynomial.

However, the LS loss given in (3) may be problematic at the presence of large outliers in the sequence data, because only the second-moment of error is used [32]. Although this problem can be solved to some extent by adjusting the window length and polynomial order, this will inevitably increase the computational burden and the cost of debugging parameters. Hence, in this study, the SG-GCL model is developed by employing GCL [31] instead of the LS loss in original SG filter aiming to enhance its stability against outliers.

Combining (1)-(3), we can defined a novel loss as

$$J_{SG-GCL} = 1 - \frac{1}{2m+1} \sum_{l=-m}^m \exp\left(-\left|\frac{\sum_{k=0}^n a_k l^k - c_l}{\sigma}\right|^\alpha\right). \quad (4)$$

Similarly, taking the derivative of (4) with respect to the coefficients and setting the derivatives to zero yields the coefficient matrix of the SG-GCL as

$$\begin{aligned} \frac{\partial J_{SG-GCL}}{\partial a} &= 0 \\ \Rightarrow \frac{\alpha}{\sigma^\alpha} \sum_{l=-m}^m \exp\left(-\left|\frac{\sum_{k=0}^n a_k l^k - c_l}{\sigma}\right|^\alpha\right) \left|\sum_{k=0}^n a_k l^k - c_l\right|^{\alpha-1} l^p &= 0 \\ \Rightarrow \frac{\alpha}{\sigma^\alpha} \sum_{l=-m}^m \exp\left(-\left|\frac{\sum_{k=0}^n a_k l^k - c_l}{\sigma}\right|^\alpha\right) \left|\sum_{k=0}^n a_k l^k - c_l\right|^{\alpha-2} \sum_{k=0}^n l^{p+k} a_k &= 0 \quad (5) \\ = \frac{\alpha}{\sigma^\alpha} \sum_{l=-m}^m \exp\left(-\left|\frac{\sum_{k=0}^n a_k l^k - c_l}{\sigma}\right|^\alpha\right) \left|\sum_{k=0}^n a_k l^k - c_l\right|^{\alpha-2} l^p c_l \\ \Rightarrow \mathbf{I}^T \mathbf{\Lambda} \mathbf{a} = \mathbf{I}^T \mathbf{\Lambda} \mathbf{c} \\ \Rightarrow \mathbf{a} = (\mathbf{I}^T \mathbf{\Lambda} \mathbf{I})^{-1} \mathbf{I}^T \mathbf{\Lambda} \mathbf{c} \end{aligned}$$

where $p = 0, 1, \dots, n$. \mathbf{a} is a matrix of coefficients consisting of a_k and $\mathbf{\Lambda}$ is a diagonal matrix whose diagonal element is

$$\Lambda_{ll} = \frac{\alpha}{\sigma^\alpha} \exp\left(-\left|\frac{\sum_{k=0}^n a_k l^k - c_l}{\sigma}\right|^\alpha\right) \left|\sum_{k=0}^n a_k l^k - c_l\right|^{\alpha-2}. \quad (6)$$

After the introduction of the diagonal matrix of (6), the larger the output error due to data noise, the smaller the values of the elements in the corresponding positions of the coefficient matrix will be, so that the influence of noise on the output results will be reduced. The solution in (5) is a fixed-point equation, and the optimal solution can be solved using a

fixed-point iterative algorithm, as shown in Algorithm 1.

Remark: The presence of outliers can make the error term result larger. The effect of outliers on (4) is limited to some extent by putting the error term into an exponent that can achieve a suppression effect on the outliers, and thus this characteristic imbues the proposed method with robust stability. In addition, we know that the HF with higher correlation with SOH can be extracted from the data closer to the real data, and the high correlation HF is the prerequisite for the accurate estimation of SOH using the data-driven method. Therefore, the preprocessing (filtering) of the measurement data using SG-GCL will be considered in our work to improve the validity of the extracted HF in order to promote stability and accuracy of the estimation model under the real situation.

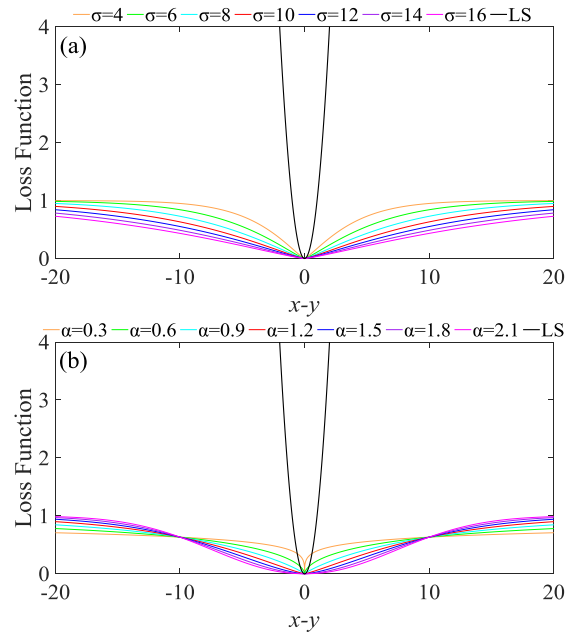


Fig. 2. Comparison of GCL and LS losses for different parameters. (a) $\alpha=1.2$ for GCL and LS. (b) $\sigma=10$ for GCL and LS.

Algorithm 1 SG-GCL.

Input: samples $\{c_l\}_{l=-m}^m$

Output: coefficient matrix \mathbf{a}

Parameters setting: polynomial order k , window length $2m+1$, shape parameter α , scale parameter σ , maximum iteration number Q_1 and termination tolerance ϵ

Initialization: set $\mathbf{a}_0 = 0$

1. **for** $q = 1, 2, \dots, Q_1$ **do**
2. Compute the error based on \mathbf{a}_{q-1} :

$$e_l = \sum_{k=0}^n a_{k,q-1} l^k - c_l$$

3. Compute the diagonal matrix $\mathbf{\Lambda}$ based on (6)
4. Update the coefficient matrix \mathbf{a} :

$$\mathbf{a}_q = (\mathbf{I}^T \mathbf{\Lambda} \mathbf{I})^{-1} \mathbf{I}^T \mathbf{\Lambda} \mathbf{c}$$

-
5. **Until** $|J_{SG-GCL}(\mathbf{a}_q) - J_{SG-GCL}(\mathbf{a}_{q-1})| < \varepsilon$
6. **end for**
-

C. Extreme Learning Machine with GCL

The traditional ELM [36] is trained by minimizing the LS loss between the actual labeled value $\mathbf{Y} = [y_1, y_2, \dots, y_N]^T$ and estimated value $\hat{\mathbf{Y}}$, while a regularization term with a penalty factor of λ is usually introduced to prevent model overfitting. The function with respect to the output weight matrix β can be expressed as

$$J_{ELM}(\beta) = \|\mathbf{Y} - \hat{\mathbf{Y}}\|^2 + \lambda \|\beta\|^2 = \|\mathbf{Y} - \mathbf{H}\beta\|^2 + \lambda \|\beta\|^2 \quad (7)$$

where $\mathbf{H} = [\mathbf{h}_1(\mathbf{x}_1), \mathbf{h}_2(\mathbf{x}_2), \dots, \mathbf{h}_N(\mathbf{x}_N)]^T$ denotes the hidden layer output matrix, $\mathbf{h}(\cdot)$ represents the activation function, and $\mathbf{X} = [\mathbf{x}_1, \mathbf{x}_2, \dots, \mathbf{x}_N]$ denotes the input matrix, which in this article denotes the matrix consisting of HFs.

By taking the derivative of (7) with respect to β and letting the derivative be equal to zero one obtains

$$\begin{aligned} \frac{\partial J_{ELM}(\beta)}{\partial \beta} &= 0 \\ \Rightarrow \beta &= (\mathbf{H}^T \mathbf{H} + \lambda \mathbf{I})^{-1} \mathbf{H}^T \mathbf{Y}. \end{aligned} \quad (8)$$

In the same way as the idea of improving the SG filter, the GCL is substituted for the loss function of the conventional ELM to develop the GELM model. Specifically, through the combination of (1), (2) and (7), it can be defined the following loss

$$J_{GELM}(\beta) = 1 - \frac{1}{N} \sum_{i=1}^N \exp\left(-\left|\frac{y_i - \mathbf{h}_i \beta}{\sigma}\right|^\alpha\right) + \lambda \|\beta\|^2. \quad (9)$$

Differentiating (9) with respect to β and letting the derivative equal zero yields the output weight matrix of the GELM as

$$\begin{aligned} \frac{\partial J_{GELM}(\beta)}{\partial \beta} &= 0 \\ \Rightarrow -\sum_{i=1}^N \frac{\alpha}{\sigma^\alpha} \exp\left(-\left|\frac{y_i - \mathbf{h}_i \beta}{\sigma}\right|^\alpha\right) (y_i - \mathbf{h}_i \beta)^{\alpha-1} \mathbf{h}_i^T &+ 2N\lambda\beta = 0 \\ \Rightarrow \sum_{i=1}^N \frac{\alpha}{\sigma^\alpha} \exp\left(-\left|\frac{y_i - \mathbf{h}_i \beta}{\sigma}\right|^\alpha\right) (y_i - \mathbf{h}_i \beta)^{\alpha-2} \mathbf{h}_i^T \mathbf{h}_i \beta &+ 2N\lambda\beta = 0 \\ = \sum_{i=1}^N \frac{\alpha}{\sigma^\alpha} \exp\left(-\left|\frac{y_i - \mathbf{h}_i \beta}{\sigma}\right|^\alpha\right) (y_i - \mathbf{h}_i \beta)^{\alpha-2} \mathbf{h}_i^T y_i & \\ \Rightarrow (\mathbf{H}^T \Lambda \mathbf{H} + 2N\lambda)\beta &= \mathbf{H}^T \Lambda \mathbf{Y} \\ \Rightarrow \beta &= (\mathbf{H}^T \Lambda \mathbf{H} + 2N\lambda)^{-1} \mathbf{H}^T \Lambda \mathbf{Y} \end{aligned} \quad (10)$$

where Λ a diagonal matrix, and the diagonal elements of Λ can be expressed as

$$\Lambda_{ii} = \frac{\alpha}{\sigma^\alpha} \exp\left(-\left|\frac{y_i - \mathbf{h}_i \beta}{\sigma}\right|^\alpha\right) (y_i - \mathbf{h}_i \beta)^{\alpha-2}. \quad (11)$$

Then the fixed-point iterative process of the GELM can be summarized in Algorithm 2.

Algorithm 2 GELM.

Input: samples $\{\mathbf{x}_i, y_i\}_{i=1}^N$

Output: weight vector β

Parameters setting: number of hidden nodes n , penalty factor λ , maximum iteration number Q_2 , shape parameter α , scale parameter σ , and termination tolerance ε

Initialization: set $\beta_0 = 0$

1. **for** $q = 1, 2, \dots, Q_2$ **do**
 2. Compute the error based on β_{q-1} : $e_i = y_i - \mathbf{h}_i \beta_{q-1}$
 3. Compute the diagonal matrix Λ based on (11)
 4. Update the coefficient matrix β :
- $$\beta_q = (\mathbf{H}^T \Lambda \mathbf{H} + 2N\lambda)^{-1} \mathbf{H}^T \Lambda \mathbf{Y}$$
5. **Until** $|J_{GELM}(\beta_q) - J_{GELM}(\beta_{q-1})| < \varepsilon$
 6. **end for**
-

III. EXPERIMENTAL DATA

This section describes the two datasets used in this article to validate the effectiveness of the proposed method. One is an LIB aging dataset obtained after nearly a year of experimentation in our Lab, and the other is a publicly available dataset from the University of Maryland [37].

The LIB used in the experiment is NCR18650GA, which makes use of lithium cobalt oxide as the positive electrode and a highly-crystallized specialty carbon as the negative electrode. The electrolytic fluid used in this LIB is an organic solvent, carefully optimized for the specialty carbon material. The battery features a spiral structure with four layers, including a cobalt acid lithium activated positive electrode, a specialty carbon-activated negative electrode, and a separator. These components are intricately arranged in a spiral pattern and stored in a protective case to ensure the battery's stability and integrity. The specifications of the LIB are shown in TABLE I and detailed information can be obtained on the website [38]. The experimental bench as shown in the Fig. 3(a) is used to carry out the aging test, which mainly consists of a battery tester that performs charging and discharging operations on the battery, a controller that sends and receives control commands and caches data, and a host computer that performs interactive operations and displays data. TABLE II outlines the working conditions of the four LIBs, which involved a charging process from CC to CV, followed by a 15-minute rest period. Subsequently, the LIBs were discharged at CC and rested for over 1.5 hours before repeating the cycle. In order to introduce greater realism to the test environment and account for variations in real-world conditions, the experiment chooses to expose the LIB to the surrounding environment, and the experimental conditions are adjusted accordingly to reflect changes in environmental conditions. The sampling frequency of the data is 1Hz, and the

capacity aging curves of the four LIBs are shown in Fig. 3(b).

TABLE I

SPECIFICATION OF EXPERIMENTAL LIB

Parameter	Value
Rated capacity	3.30Ah
Nominal voltage	3.60V
Maximum voltage	4.25V
Discharge cutoff voltage	2.50V
Maximum discharge current	3.00C

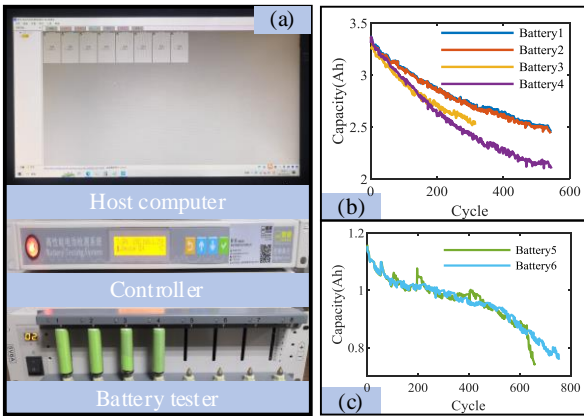


Fig. 3. Battery aging test and trajectory. (a) Test bench. (b) NCR18650GA dataset. (c) Maryland dataset.

In the University of Maryland dataset [37], data from two prismatic batteries with a rated capacity of 1.1Ah are selected. They are CS2-35 (battery5) and CS2-37 (battery6), and they have a charging cutoff current of 0.05 A and a discharging cutoff voltage of 2.7 V. The test conditions of these two batteries are given in TABLE II. The corresponding capacity aging curves are shown in Fig. 3(c).

As can be seen from Fig. 3(b)-(c), even under the same working conditions, the aging rate of the same type of battery will be different due to cell-to-cell inconsistency. Under different working conditions, the difference in aging rate of the same type of battery becomes even more pronounced. In addition, the aging trend and rate of different types of batteries demonstrate much higher level of deviation. This implies that the selection of the HFs may vary according the type of the battery.

TABLE II

CHARGING AND DISCHARGING WORKING CONDITION OF EXPERIMENTAL LIBS

Battery	Charge stage			Discharge stage	
	CC	CV	Cutoff current	CC	Cutoff voltage
battery1	0.5C	4.2V	0.01C	1.0C	2.5V
battery2	0.5C	4.2V	0.01C	1.0C	2.5V
battery3	0.8C	4.2V	0.01C	1.0C	2.5V
battery4	0.5C	4.2V	0.01C	1.5C	2.5V
battery5	0.5C	4.2V	0.05A	1.0C	2.7V
battery6	0.5C	4.2V	0.05A	1.0C	2.7V

IV. RESULTS AND ANALYSIS OF DATA PROCESSING

To achieve accurate SOH estimation based on extracted HF, it is crucial to reduce the influence of noise generated in the feature extraction process. In this section, experimentally measured and available aging data are analyzed and discussed. The HF extraction results for different battery models are

given to investigate the effect of different filtering algorithms under non-Gaussian noise with outliers. This section corresponds to our proposed SOH estimation framework including the 'SG-GCL filtering' and 'HFs extraction' parts as shown in Fig. 1.

A. Data Filtering

It should be noted that the sampling frequency for battery5 and battery6 differs from the 1Hz as used for other batteries. This may cause larger errors in the subsequent HF extraction. To solve this problem, the two sets of battery data are first interpolated.

Generally, the collected measurement data collected by sensors may be contaminated by measurement noise with outliers, and this fact is verified by experimentally collected data as shown in Fig. 4(a). One can observe from Fig. 4(a) that the distribution and magnitude of noise in the current and voltage curves for one charging cycle are random. Furthermore, the presence of non-Gaussian noise in the collected data is also illustrated in [39]. In order to verify the effectiveness and advantages of the improved method, artificially simulated non-Gaussian noise with outliers is added to all the collected data. Comparisons are also made with the original SG filter, MA filter and Gaussian filter (GF) [41].

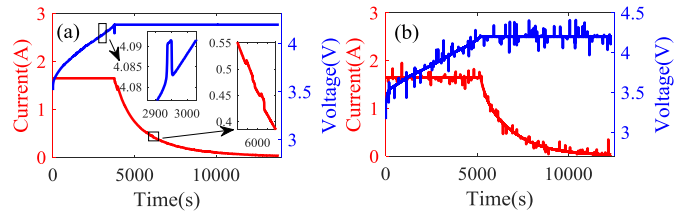


Fig. 4 Noisy data. (a) Experimentally collected data. (b) Artificially noisy data.

The model of the non-Gaussian noise superimposed with background noise and a certain percentage of outliers is defined as

$$\text{noise_NG} = \text{noise_B} + \text{noise_O} \quad (12)$$

where *noise_B* represents background noise, and *noise_O* denotes outlier noise. Both sub-noises are determined by setting the mean and variance. The non-Gaussian noise details used in the next three cases are displayed in TABLE III.

TABLE III

COMPOSITION OF NON-GAUSSIAN NOISE IN EACH CASE

	Background noise	Outlier noise	Outlier ratio
Case1	Uniform	Gaussian	1%
Case2	Gaussian	Gaussian	1%
Case3	Uniform	Gaussian	3%

A group of data processed with added noise is shown in Fig. 4(b). It should be noted that for all the collected data, the noises are generated by randomization. Thus, the noises added to each acquired data curve are different. In addition, this study increases both the frequency and the magnitude of the noise in order to better demonstrate the effectiveness of proposed method and the variability of different methods. For the setting of parameters, the filter window lengths for SG-GCL, SG, MA and GF in each case are $2m+1=91$. The fitted

polynomial order $n=2$ for SG-GCL and SG. The parameters $\alpha=1.2$ and $\sigma=10$ for SG-GCL. Root mean square error (RMSE) [40] is used to quantify the filtering effect.

$$\text{RMSE} = 100\% \times \sqrt{\frac{1}{N} \sum_{i=1}^N (\text{error}_i)^2} \quad (13)$$

where *error* denotes the absolute error between filtering result and actual value for each filtering method.

Case1: Mixed uniform and Gaussian noise with 1% outliers

In this case, the mean of the uniform noise is 0 and the variance is 3.3333e-7. Usually, the number of outliers might be smaller compared to the rest of the data in training set, and thus the Gaussian noise has a mean of 0 and a variance of 0.1 to model the outliers in this case. The filtering results of current and voltage are respectively presented in Fig. 5 and 6. The widths of the error bars in the relative error plots for current and voltage are 0.05 and 0.001, respectively. Taking an overall perspective of the two sets of figures, all four methods achieve some level of noise reduction. When observing the local details in Fig. 5(a)-(d) and 6(a)-(d), one can see that the SG-LS exhibits poorer performance compared to SG-GCL when outliers are present due to the severe impact of outliers on the loss function of SG-LS. As is well known, the MA is based on the principle of computing the arithmetic mean within the calculation window, therefore the presence of outliers causes an overall shift in the numerical values within the window. The length of this shifted data sequence is influenced by both the window length and the nature of the outliers. Analyzing the relative error distribution (RED) shown in Fig.5 (e)-(h), one can observe that the filtering relative error of SG-GCL is more concentrated around zero. This result indicates that the filtering outcomes of SG-GCL exhibit a higher number of points in close proximity to the actual value, aligning with the desired in data filtering. And the filtering results of the GF demonstrate similar local properties with the SG-LS.

Additionally, TABLE IV provides an overview of the computational efficiency of the four filtering methods in terms of the required filtering time. It is worth noting that the SG-GCL exhibits the highest time complexity due to the incorporation of fixed-point iterations. However, on the one hand, the experiments in the article involve filtering of complete charging data to better demonstrate the advantages of the methods in terms of filtering accuracy and stability. It is important to highlight that future work can focus on extracting HF from local curves and filtering only the charging data corresponding to HF, which may lead to potentially improved computational efficiency. On the other hand, the estimation of SOH does not require high real-time requirements relative to

State of Charge (SOC), and it only needs to be calculated automatically when the device is idle. As mentioned above, the time complexity of SG-GCL can be adjusted artificially and is deemed acceptable in relation to the performance improvement it brings.

Case2: Mixed Gaussian and Gaussian noise with 1% outliers

In this case, different non-Gaussian noises are further considered compared to Case1 to validate the stability of SG-GCL against different noise distributions. Here Gaussian noise with zero mean and variance of 0.001 is used as background noise, while Gaussian distribution with zero mean and variance of 0.1 is used to model outliers. The filtering results of current and voltage are respectively presented in Fig. 7 and 8. From Fig. 7(a)-(d) and 8(a)-(d), it can be seen that SG-GCL still exhibits the best local performance. SG-LS, MA and GF still show the same drawbacks as in Case 1. From Fig. 7(e)-(h) and 8(e)-(h), it can be observed that compared to SG-LS, the relative error of SG-GCL is more concentrated. From the RED of MA in Fig.7 (g) and Fig.8 (g), one can see that there is also a slight aggregation at non-zero points apart from the aggregation at 0. This is because MA is influenced by outliers, leading to an overall shift of filtered data away from the actual data. Moreover, under the same filtering parameters, the proposed SG-GCL still maintains very low filtering error, which reflects its stability.

Case3: Mixed uniform and Gaussian noise with 3% outliers

In this case, the numerical experiment is performed under the same noise conditions as in Case 1 with the difference being that the proportion of outlier noise increased to 3% to evaluate the robustness of the proposed method. The filtering results of current and voltage are respectively shown in Fig. 9 and 10. One can observe from Fig. 9 and 10 that there is no significant change observed in the filtering effect, both overall and locally. In addition, comparing the RED plot with Case1, it is found that under the condition where non-Gaussian noise does not obscure the original signal information, there is no clear relationship between filtering error variation and the proportion of outliers. The reason behind the aforementioned results is that all four methods are local filtering algorithms, and their filtering effectiveness is only related to the data within the filtering window and their own parameter settings, rather than the overall distribution of the data. Moreover, the collected charging data is difficult to conform to a specific distribution because of the high dependence of battery charging and discharging data integrity on user charging habits. Therefore, this is one of the reasons why local filtering algorithms are chosen in this study.

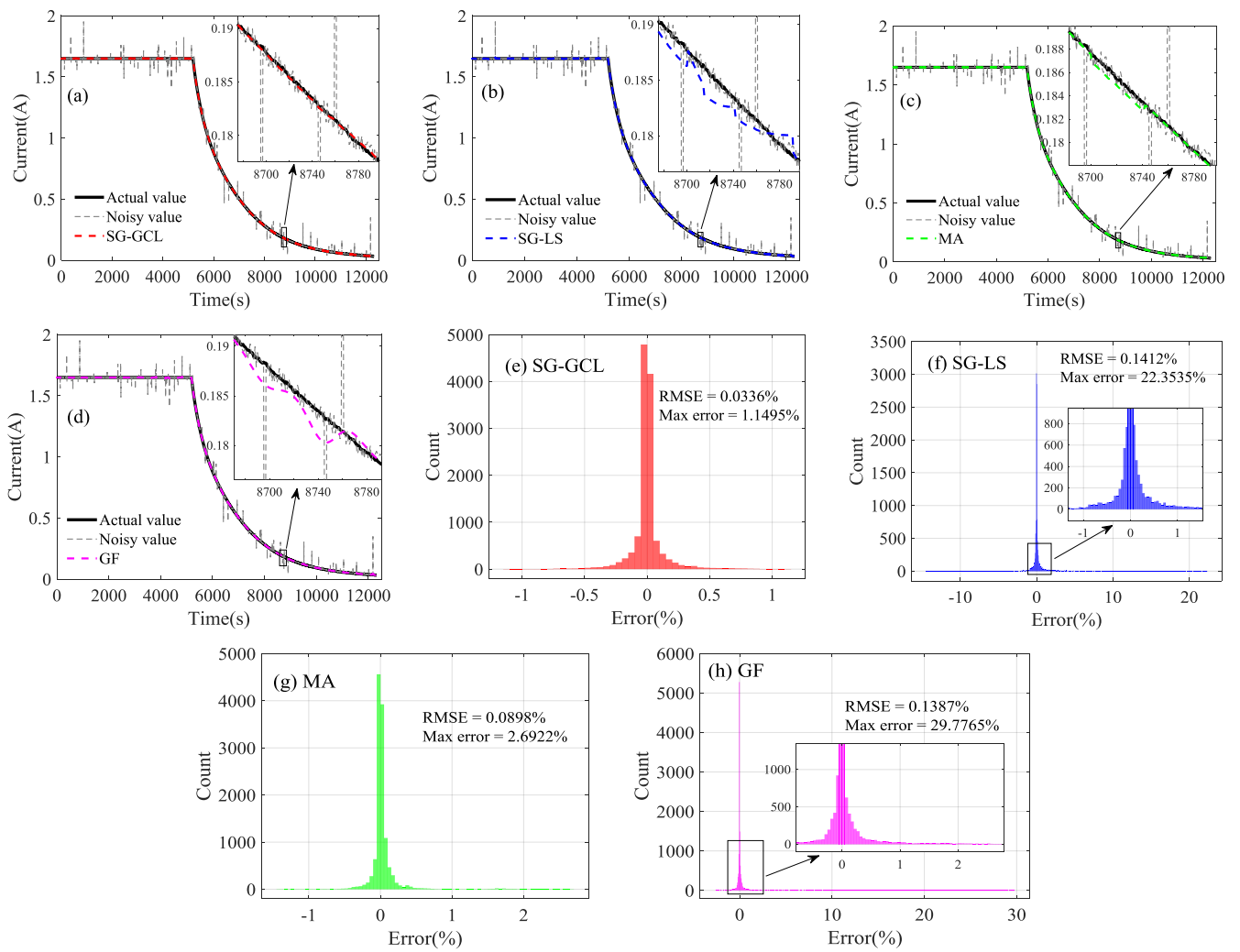
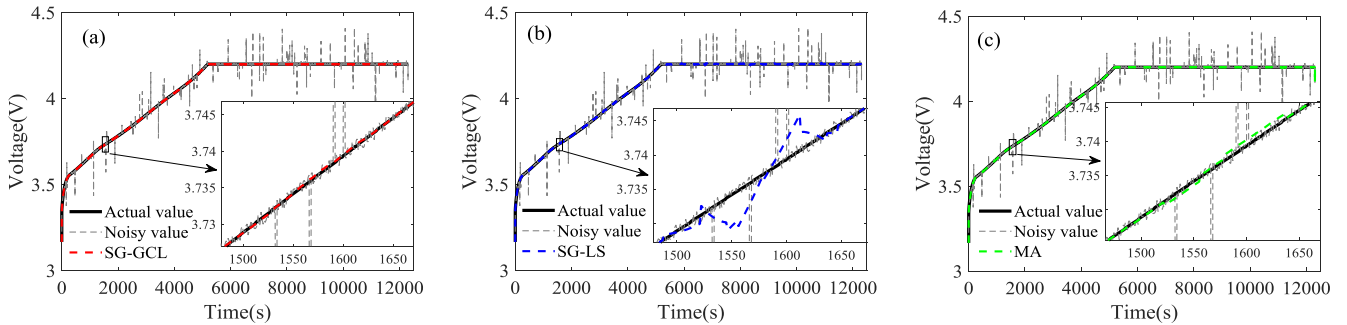


Fig. 5. Comparison of current filtering results for case1. (a)-(d) Current filtering results. (e)-(h) Relative error distribution.



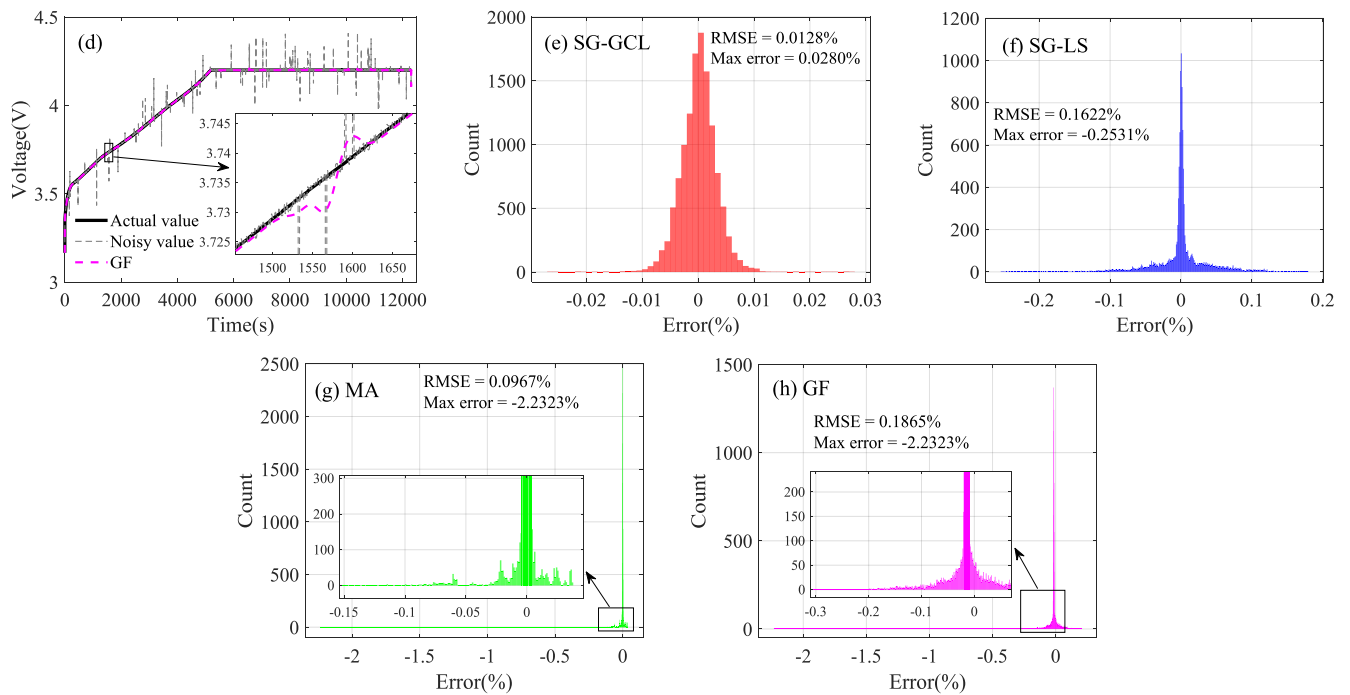


Fig. 6. Comparison of voltage filtering results for case1. (a)-(d) Voltage filtering results. (e)-(h) Relative error distribution.

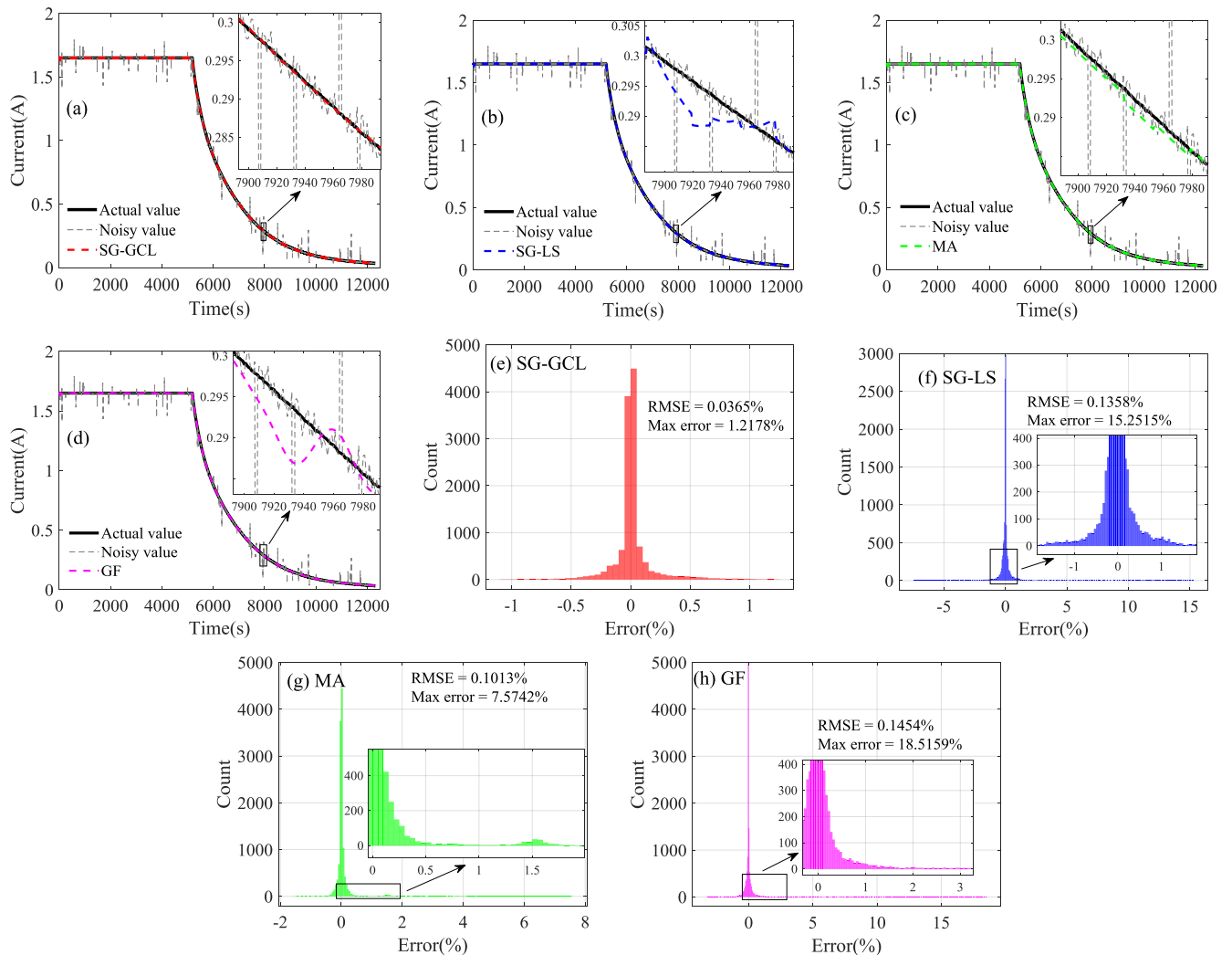


Fig. 7. Comparison of current filtering results for case2. (a)-(d) Current filtering results. (e)-(h) Relative error distribution.

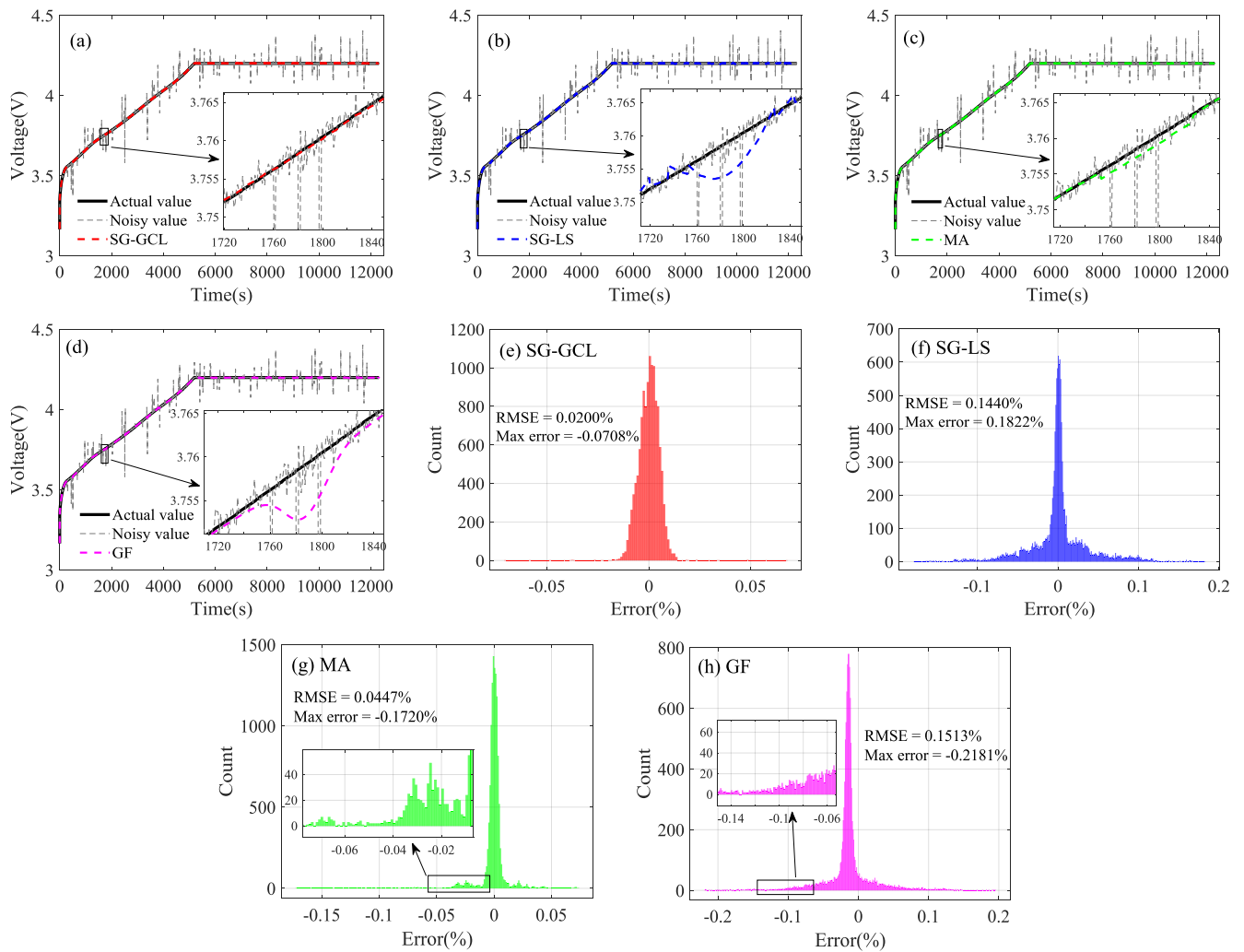
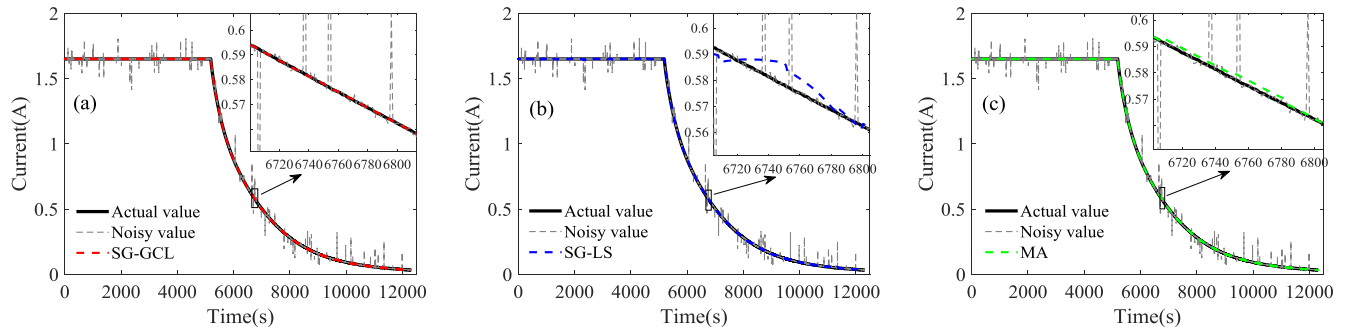


Fig. 8. Comparison of voltage filtering results for case2. (a)-(d) Voltage filtering results. (e)-(h) Relative error distribution.



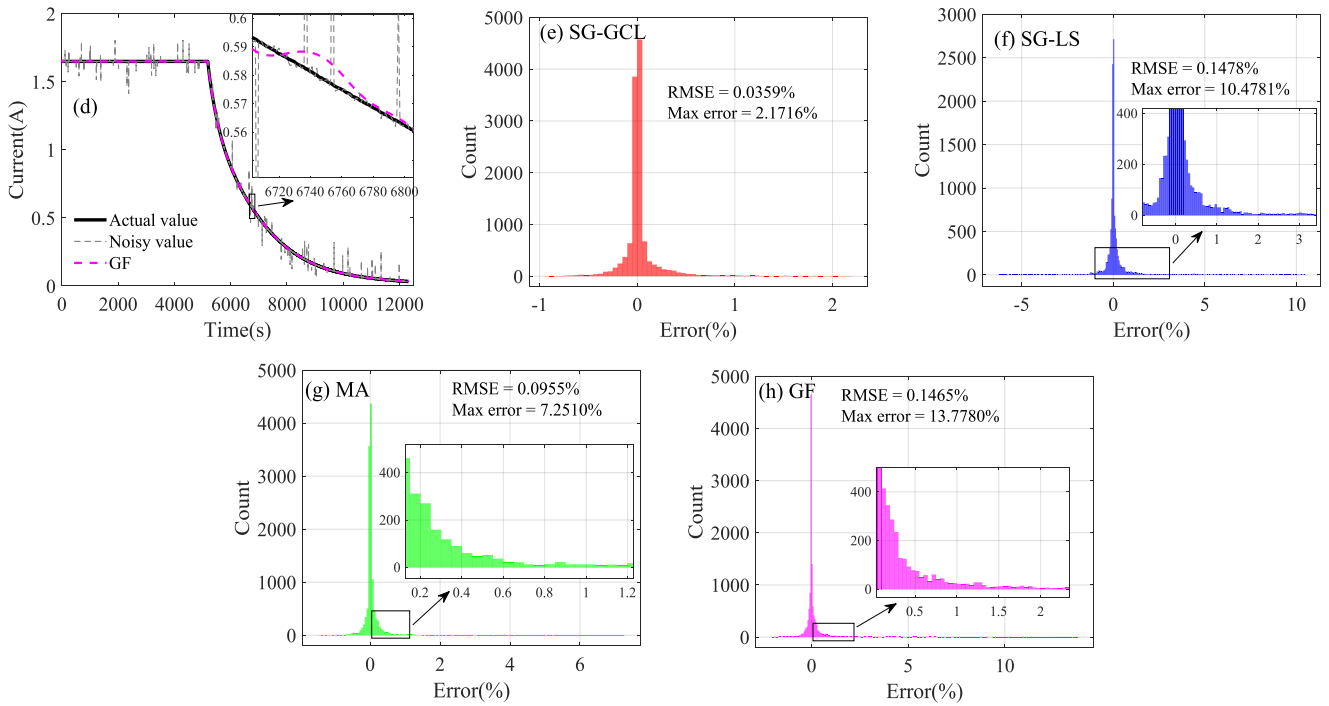


Fig. 9. Comparison of current filtering results for case3. (a)-(d) Current filtering results. (e)-(h) Relative error distribution.

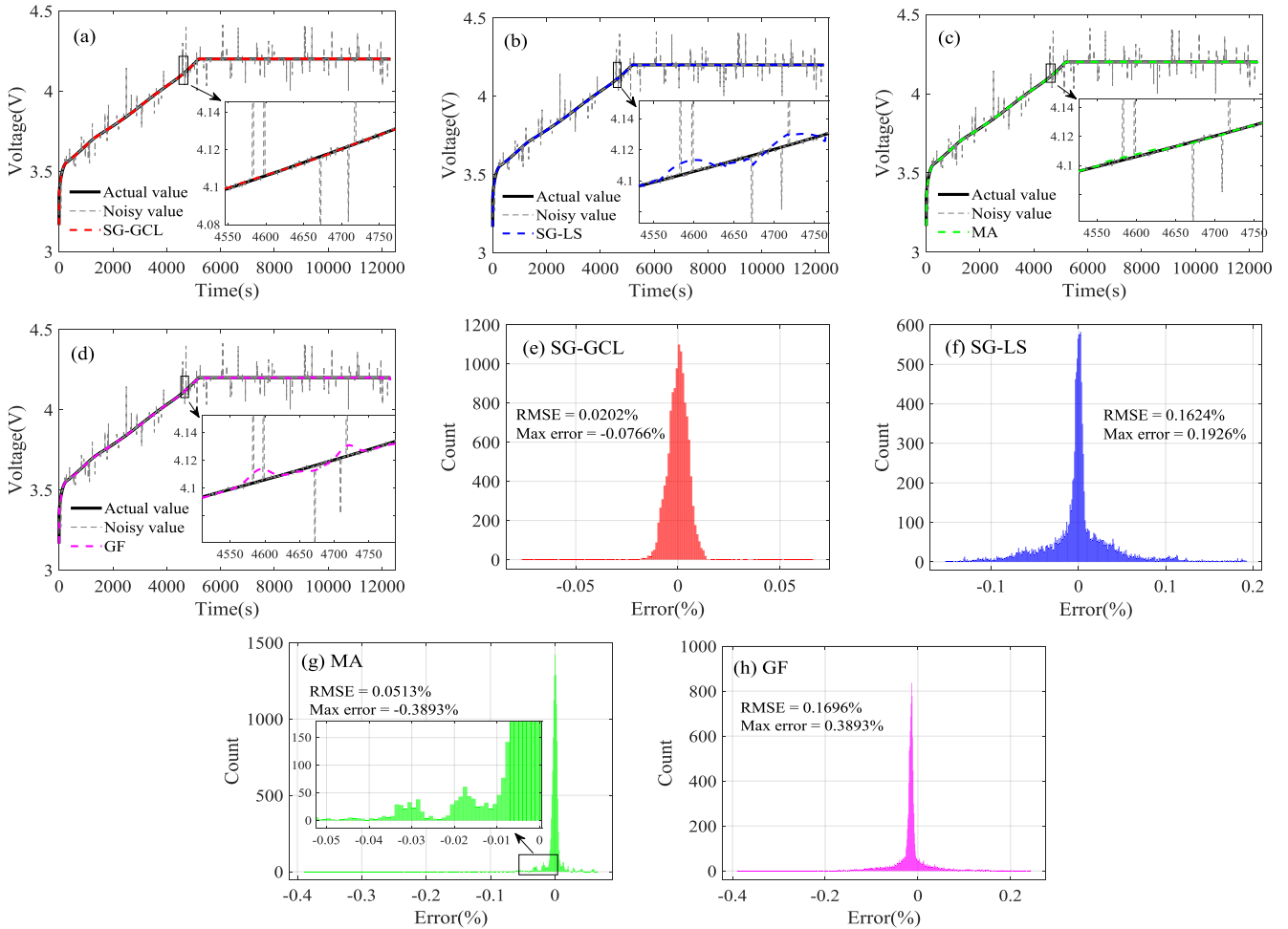


Fig. 10. Comparison of voltage filtering results for case3. (a)-(d) Voltage filtering results. (e)-(h) Relative error distribution.

> REPLACE THIS LINE WITH YOUR MANUSCRIPT ID NUMBER (DOUBLE-CLICK HERE TO EDIT) <

TABLE IV
TIME COMPLEXITY OF DIFFERENT METHODS

	SG-GCL	SG-LS	MA	GF
Filter time	39.53s	0.09s	0.02s	0.01s

Based on the results of the above three cases, it can be seen that no matter how the noise distribution and quantity change, the proposed SG-GCL can show satisfactory filtering effect under the condition of constant parameters, reflecting good stability. Compared with SG-GCL, SG-LS shows obvious short-term and significant fluctuations, while MA shows long-term and smaller fluctuations. The classical GF also exhibits more similar characteristics to SG-LS, reflecting the limitation of traditional filters when facing non-Gaussian noise. These findings demonstrate that the SG-GCL can still effectively adapt to different distributions of noise while maintaining stable and robust filtering performance even when the parameters are not frequently adjusted.

B. HF Extraction and Correlation Analysis

The charging time of different charging stages at different aging levels has been shown to be highly correlated with battery aging [41]. Therefore, in this article, the time-dependent HF is extracted directly from the current and voltage curves of the filtered charge. For the CC stage, on the one hand, the [3.75V, 4.2V] interval of the voltage curve is divided into multiple voltage segments, and the charging duration of each voltage interval is taken as the HF. On the other hand, different starting voltages and charging time intervals are set, and the value of the voltage increase within this time interval is taken as the HF. At the same time, the current curve of CV stage also follows this idea. The current curve of CV stage is firstly divided into several current segments in the interval of [0.55A, 0.15A], and the charging time of each segment is taken as HF, and then different starting currents and charging time intervals are set, and the current reduction value in a certain time interval at a specific starting current is taken as HF. Based on this approach, 82 different HFs are extracted. A screening processing is needed to reduce the number of HFs for the use of SOH estimation.

To evaluate the compatibility of the extracted HFs, all HFs are subjected to Pearson correlation analysis (PCA) [42] with the capacity separately. The PCA between sample pairs $\{(x_i, y_i)\}_{i=1}^n$ can be calculated as follows.

$$pearson = \frac{\sum_{i=1}^n (x_i - \bar{X})(y_i - \bar{Y})}{\sqrt{\sum_{i=1}^n (x_i - \bar{X})^2} \sqrt{\sum_{i=1}^n (y_i - \bar{Y})^2}} \quad (14)$$

where \bar{X} and \bar{Y} denote the mean of the two samples, respectively.

After performing the correlation analysis, it is interesting to find that it is possible that the correlation of the same HF with capacity varies significantly for the same type of cell under different operating conditions. Specifically, a HF showing a very high correlation with capacity in one battery can have a

very low correlation with capacity in another battery. This phenomenon is even more pronounced between different types of batteries. Based on the results of PCA, seven HFs are chosen for each battery. The absolute values of the PCA between these HFs and SOH are all greater than 0.97, with four positive correlations and three negative correlations. The HFs under the two datasets are shown in Fig. 11. They characterize the charging duration and the current drop or voltage rise over a certain period of time in the current or voltage interval, respectively. Another representation of the extracted HFs is provided in TABLE V. In this study, measures have been taken to ensure the consistency of the HFs within the same dataset. However, it is difficult to maintain the consistency of the HFs extracted from different datasets. The used HFs and capacities are normalized before the SOH estimation experiments.

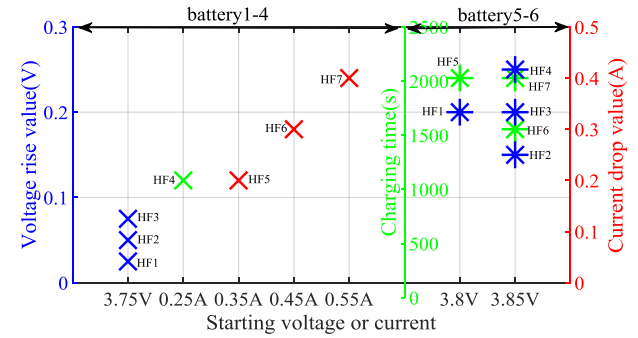


Fig. 11. HF extracted for each battery.

TABLE V

BATTERY HFs

HF	battery1-4		battery5-6	
	Start value	Interval	Start value	Interval
HF1	3.75V	0.025V	3.80V	0.20V
HF2	3.75V	0.050V	3.85V	0.15V
HF3	3.75V	0.075V	3.85V	0.20V
HF4	0.25A	1000s	3.85V	0.25V
HF5	0.35A	0.20A	3.80V	2000s
HF6	0.45A	0.30A	3.85V	1500s
HF7	0.55A	0.40A	3.85V	2000s

Illustrating with battery1 as a case study, Fig.12 depicts the extracted HF1 obtained from filtering the measurement data using various filtering data. Considering the similarity of the GF and SG-LS filtering results and the observability of the figures, the comparison of the GF method is subsequently cancelled. Notably, the HF extracted from the measurement data filtered by SG-GCL exhibits superior stability, with relatively small fluctuations over cycle. Comparatively, the SG-GCL shows a significant enhancement in feature extraction when compared to SG-LS. And the feature extraction results produced by MA are generally satisfactory in this specific instance. However, a significant deviation occurs at the 482nd point, which is attributed to the limitations of MA discussed in section IV.A. The presence of a certain offset in MA filtering within a specific interval can lead to substantial deviations between the extracted HF points and the actual values, particularly when the sampling points of HF fall within this interval. Additionally, extracting HF data without

> REPLACE THIS LINE WITH YOUR MANUSCRIPT ID NUMBER (DOUBLE-CLICK HERE TO EDIT) <

filtering the measurements containing noise will significantly reduce the amount of aging information captured. This can be illustrated by the 'None' curve in Fig. 12, which displays numerous offset points that obscure the actual data information. The correlation between the HF extracted by the four methods after processing and the SOH is provided in TABLE VI. Numerically, it is more evident that the HF extracted from the measurement data processed by SG-GCL exhibits the highest correlation with SOH, whose PCA result is higher than that of SG-LS, MA and None by 0.0834, 0.0305 and 0.4963, respectively, indicating the superior performance. These results further underscore the advantages of employing the SG-GCL filtering algorithm.

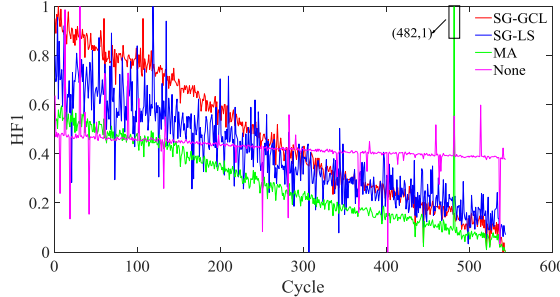


Fig. 12. HF1 extraction results of battery1 after processing by different filtering methods.

TABLE VI
PCA FOR HF1 OF BATTERY1

	SG-GCL	SG-LS	MA	None
HF1	0.9829	0.8995	0.9524	0.4866

V. EXPERIMENTAL RESULTS FOR SOH ESTIMATION

In this section, the proposed method is verified using three illustrative cases in following subsections. The data used in each of the three subsections are given in TABLE VII. The experiment consists of three main sections, each comprising two sub-experiments. In each sub-experiment, the model undergoes training and testing stage. All battery current and voltage data are processed in Section IV. The processing of battery SOH label values in the training data will be presented in the subsequent experiments. The SOH label values of the test data are used to calculate the model evaluation metrics and to assess the model estimation accuracy. During the training phase, the battery data is comprised of HFs-label value pairs, with data from multiple batteries concatenated if multiple batteries are used for training. Conversely, only the battery's HFs are inputted during the testing phase. This section corresponds to the proposed SOH estimation including 'GELM training' and 'SOH estimation with GELM' parts as shown in Fig. 1.

TABLE VII
EXPERIMENTAL DATA

Section	Training data	Test data
V.A	battery1, battery3, battery4	battery2
	battery1, battery2, battery3	battery4
V.B	battery6	battery5
	battery5	battery6
V.C	battery2, battery3, battery4	battery1

battery1, battery2, battery4 battery3

In the following experiments, the RMSE of (13) and mean absolute percentage error (MAPE) [40] are mainly used to evaluate the SOH estimation accuracy of the model, and the MAPE is defined as

$$\text{MAPE} = \frac{100\%}{N} \times \sum_{i=1}^N \left| \frac{y_i - \hat{y}_i}{y_i} \right| \quad (15)$$

where $\mathbf{y} = [y_1, y_2, \dots, y_N]$ and $\hat{\mathbf{y}} = [\hat{y}_1, \hat{y}_2, \dots, \hat{y}_N]$ denote the actual and estimated values of SOH with N sample points, respectively.

A. Validation of Filtering Algorithm

Section IV compares the filtering effects of different algorithms and their impact on the extracted HFs. This subsection further validates the necessity and effectiveness of filtering measurement data for SOH estimation. HF is extracted from the measurement data after filtering with three different filtering methods and from unfiltered data. The extracted HFs by using four processing methods including SG-GCL, SG-LS, MA and None are used to train and test the models. The corresponding four SOH estimation models are denoted as ELM-SG-GCL, ELM-SG-LS, ELM-MA, and ELM-None. To ensure a fair comparison, the number of nodes in the hidden layer of ELM is consistently set to 5 for both sets of experiments. The results of the two experiments are respectively shown in Fig. 13 and 14. In Fig. 13(a), the model trained from HF extracted directly from the noise-laden measurement data exhibits considerable estimation inaccuracies, with notable deviation from the true SOH value. This further emphasizes the crucial importance of applying suitable filtering techniques on measurement data. And the relative error number distribution plots in Fig. 13(b)-(e) show that ELM-SG-GCL exhibits concentrated error results, with a prominent concentration of errors close to zero. Compared with ELM-SG-GCL, the relative errors of the other three model estimation results are more dispersed, which indicates the larger deviation of their estimation results relative to the real SOH. The estimation results shown in Fig. 14 are more pronounced. In Fig. 14(a), the estimation results of ELM-None fluctuate significantly above and below the actual value, which is still due to the influence of the HF extracted from the measurement data affected by unknown distribution noise. Furthermore, it is evident that the estimation results of ELM-MA display small fluctuations but gradually deviate from the actual value over cycle. This discrepancy arises due to the presence of a relatively prominent outlier in the HF extracted after MA filtering, similar to the one depicted in Fig. 12. Consequently, ELM-MA is adversely affected during the training process, leading to the generation of an inaccurate model. In addition, the more apparent advantages of ELM-SG-GCL are demonstrated in Fig. 14(b)-(e). Substantiated by the centered errors approaching zero and narrower error distributions, it unmistakably showcases the superiority of SG-GCL in effectively handling measurement data characterized

> REPLACE THIS LINE WITH YOUR MANUSCRIPT ID NUMBER (DOUBLE-CLICK HERE TO EDIT) <

by unknown distribution noise. For a comprehensive analysis, TABLE VIII provides a more detailed comparison of RMSE and MAPE under various methods. Notably, ELM-SG-GCL outperforms others by consistently demonstrating the smallest estimation error, thus establishing its commendable accuracy in estimating target outcomes. More specifically, the estimated RMSE of ELM-SG-GCL for battery2 is found to be 0.49%, 0.28% and 51.99% lower than that of ELM-SG-LS, ELM-MA and ELM-None, respectively. Similarly, for battery4, the estimated RMSE of ELM-SG-GCL is 0.54%, 1.79% and 43.69% lower than that of ELM-SG-LS, ELM-MA and ELM-None, respectively. These results unequivocally demonstrate both the importance of filtering noisy measurement data and the effectiveness of the SG-GCL filtering method when it comes to accurate SOH estimation results.

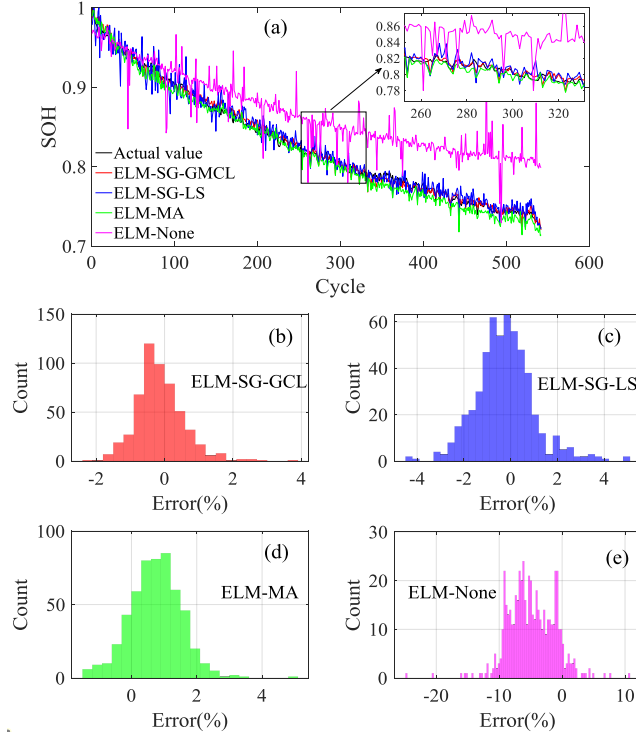


Fig. 13. Results of battery2. (a) Estimated result. (b)-(e) Relative error distribution.

B. Model Validation

In order to demonstrate the benefits of the proposed stable estimation model, this subsection further introduces non-Gaussian noise containing outliers to the labeled values of all the training data. The non-Gaussian noise is denoted as (12), with the background noise chosen as uniform noise with a mean of 0 and a variance of $3.3333\text{e-}5$, and the outlier noise as Gaussian noise with zero mean and a variance of 2. The input data for all models are HFs extracted from the data filtered by SG-GCL, and the training outputs are labeled SOH with noise. In this case, a comparative analysis between the proposed GELM proposed in section II.C and ELM to verify the effectiveness of the enhanced approach. Through a series of controlled experiments, specific parameter values are selected to ensure that each method achieves its optimum performance. For the GELM, the α is set to 5, σ is set to 0.05, and the

number of hidden layer nodes is set to 5, all informed by comprehensive iterations. Likewise, the number of hidden layer nodes for ELM is also established as 5 based on similar considerations for harmonized evaluations.

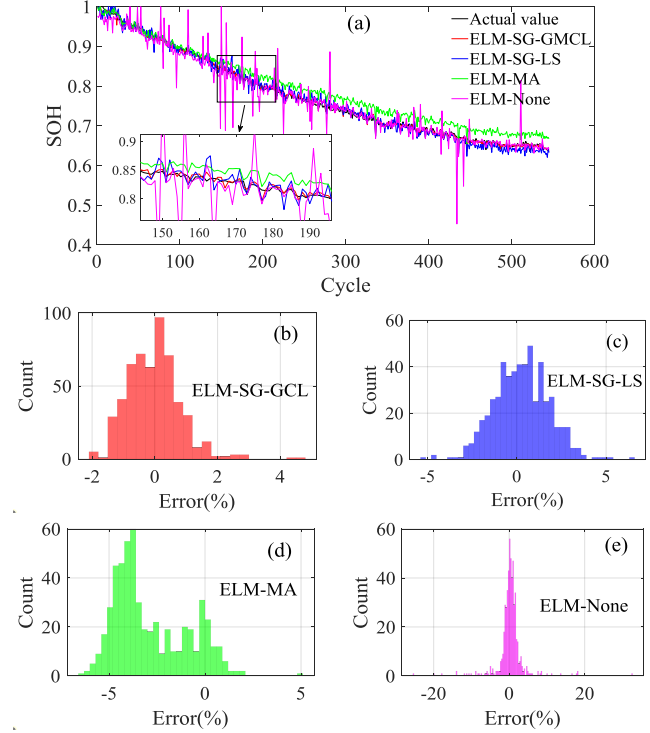


Fig. 14. Results of battery4. (a) Estimated result. (b)-(e) Relative error distribution.

TABLE VIII
ESTIMATION ERRORS OF HF IN DIFFERENT METHODS (%)

	battery2	battery4
ELM-SG-GCL	RMSE	0.60
	MAPE	0.91
ELM-SG-LS	RMSE	1.09
	MAPE	1.72
ELM-MA	RMSE	0.88
	MAPE	1.24
ELM-None	RMSE	52.59
	MAPE	64.19

The experiment results for battery5 and battery6 are represented in Fig. 15 and Fig. 16, respectively. One can see from the results that the GELM outperforms ELM when the training labeled values contain non-Gaussian noise. Specifically, for battery5 in Fig. 15(a), both models yield considerable estimate errors, but the GELM exhibits significantly smaller deviation. In Fig. 15(b), the estimation error of GELM mainly falls within the range between -2% and 0.5%, with the mean error of approximately -0.6%. In contrast, the estimation error of ELM spans from -3.5% to 0%, with the its mean around -2%. In Fig. 16(a), the GELM again shows a superior fit compared to the base model ELM. Examining the error distribution of Fig. 16(b), the error center of GELM stays around 0.6%, which demonstrates a more centralized error compared to ELM. The error of ELM is dispersed almost evenly between -2% and 3%, indicating a high degree of variability. Comparing Fig. 15 with Fig. 16,

> REPLACE THIS LINE WITH YOUR MANUSCRIPT ID NUMBER (DOUBLE-CLICK HERE TO EDIT) <

there are significant differences in the estimation results when the data from two batteries are used as training sets for each other. The estimation result of battery5 is oversized, while the estimation result of battery6 is undersized. This phenomenon stems from the different distribution of HFs versus labeled values for the two batteries. TABLE IX also provides a comparison of the estimation evaluation of battery5 and battery6 under different models, where GELM shows a considerable advantage over ELM, with a numerical reduction of 0.7% in RMSE and 0.9% in MAPE for battery5, and a numerical reduction of 0.66% in RMSE and 0.74% in MAPE for battery6. Therefore, when the training label values contain outliers, the proposed GELM model demonstrates a more substantial improvement in estimation accuracy compared to the basic ELM model.

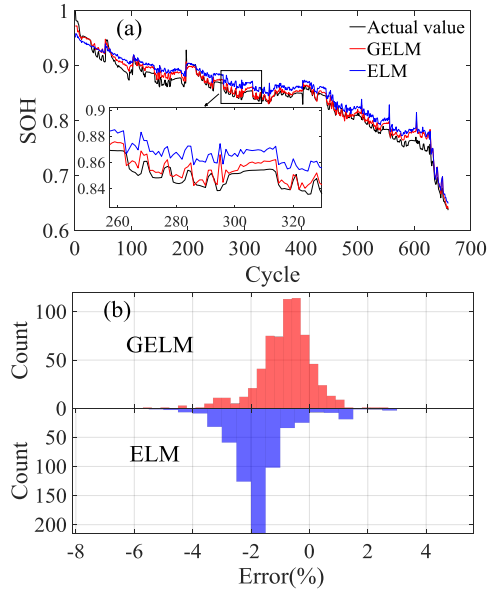


Fig. 15. Results of battery5. (a) Estimated result. (b) Relative error distribution.

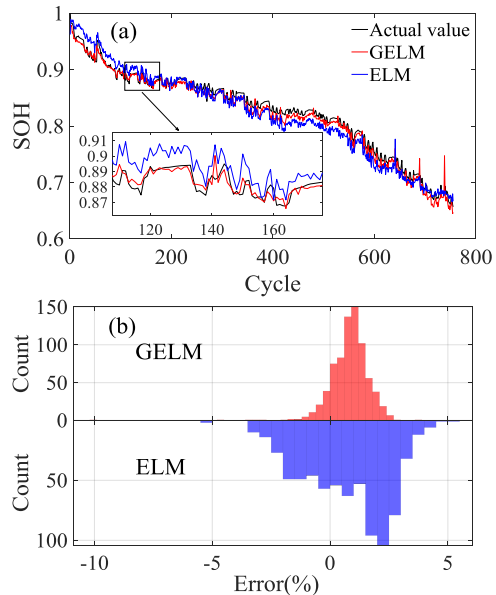


Fig. 16. Results of battery6. (a) Estimated result. (b) Relative error distribution.

TABLE IX
COMPARISON OF ERRORS (%)

	GELM		ELM	
	RMSE	MAPE	RMSE	MAPE
battery5	1.00	0.91	1.70	1.81
battery6	0.94	0.92	1.60	1.66

C. Comparison Between Different Types of Models

In this subsection, a comparative analysis is further conducted to evaluate the performance of the proposed GELM model compared with two widely used existing models, namely LSTM [25] and GPR [27]. Considering the data volume of SOH is relatively small in this case, resembling small sample sizes, too many deep network layers in LSTM could potentially lead to model overfitting. To address this, after multiple experiments, here the LSTM is configured with a single hidden layer comprising 15 nodes, limited to a maximum of 100 iterations. In the case of GPR, the parameter ‘sigma’, which significantly influences noise deviation, is set to 0.2, in line with the focus on noise related aspects in this study. The remaining parameters of both models are set to their default values. The non-Gaussian noise settings for the SOH labelled align with those in section V.B, as do the experimental conditions. It should be noted that while the noise parameter settings are consistent with section V.B, the specific noise added varies due to the random nature of noise generation and variations in data points between sections V.B and V.C. The results are presented in Fig. 17 and Fig. 18.

The comparison depicted in Fig. 17(a)-(c) showcases the superior goodness of fit achieved by the proposed GELM method in comparison to the traditional LSTM and GPR models. The estimated SOH value from GELM aligns more closely with the actual value. In contrast, the GPR model exhibits greater deviation from the actual value, particularly at the early and the middle age of the batteries. This discrepancy is even more pronounced in the case of LSTM. It is demonstrated that the two traditional models are susceptible to outliers during training, while GELM eliminates this effect to some extent. This can be more directly observed in the error from the box diagram in Fig. 17(d), where the estimation error interval of GELM is significantly smaller than that of LSTM and GPR, with the error center closer to zero and fewer outliers. Compared to the estimation results of battery1, the estimation results of battery3 in Fig. 18(a)-(c) all significantly deviate from the actual value. However, the GELM model exhibits comparatively smaller deviations than the other two models. Fig. 18(d) further illustrates a much narrower upper and lower interquartile range with no outliers beyond the upper and lower margins. The error center of the GELM is within an acceptable 1.1%. The RMSE and MAPE results for both batteries are displayed in Fig. 19. The advantage of resisting outliers GELM is also reflected in the bar results.

From the estimation results in Fig. 17(a) and Fig. 18(a), the error of battery3 increases significantly. This is attributed in part to the different noise distribution of the training data.

> REPLACE THIS LINE WITH YOUR MANUSCRIPT ID NUMBER (DOUBLE-CLICK HERE TO EDIT) <

More importantly, the absence of a dataset with the same charging and discharging conditions as battery3 in the training set contributes to a significant difference in aging distributions, resulting in a larger estimation error. However, the charging and discharging working conditions of battery4 in Section V.A are also not the same as the training set. The difference between the results of battery2 and battery4 under the same estimation model is also not as large as the difference between the estimation results of battery1 and battery3. Comparing the four charging and discharging conditions in TABLE II, it can be seen that battery3 conditions differ in the current value of CC in the charging stage, while battery4 conditions differ in the current value of CC in the discharging stage. This infers that the battery data with different charging conditions in the training and test sets have a more significant impact on the estimation accuracy, while the battery data sets with different discharging conditions have a smaller influence.

In contrast to the aforementioned DD method, here an outstanding MD method, called MCC extended Kalman filter (MCCEKF), is further introduced into the comparison experiment to test the superior performance of the proposed method. This evaluation focuses solely on the final estimation

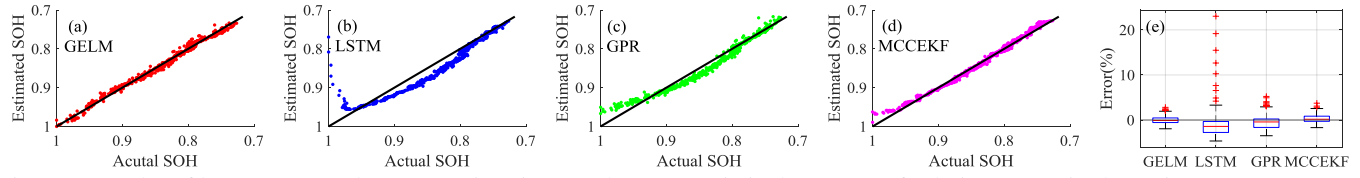


Fig. 17. Results of battery1. (a)-(d). SOH estimation results. (e) Statistical patterns of relative errors in the estimates.

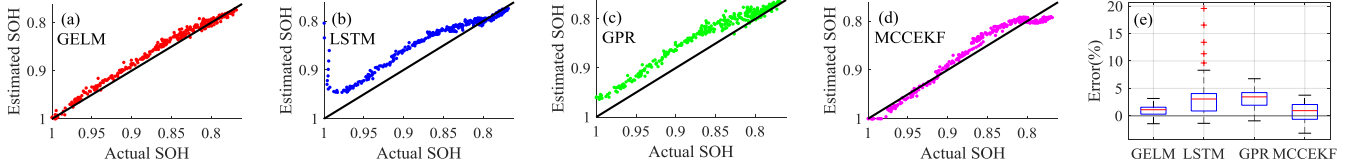


Fig. 18. Results of battery3. (a)-(d). SOH estimation results. (e) Statistical patterns of relative errors in the estimates.

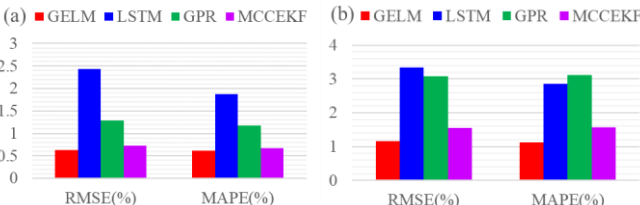


Fig. 19. Comparison of model RMSE (%) and MAPE (%). (a) Battery1. (b) Battery3.

VI. DISCUSSION

In this section, the SOH estimation framework for LIB developed in this article is further discussed. The general tone of the framework is a data-driven approach. Firstly, the unknown distributed noise in the measurement data (current, voltage) is filtered using SG-GCL. Then, the HF characterizing battery aging is extracted from the processed data. After that, the extracted HF and SOH label values are used to form a training data pair for training the introduced GELM as an estimation model. Finally, the SOH can be estimated using the newly extracted HF and the trained

performance of the models. Drawing inspiration from [30] and [43], the SOH to be estimated is fitted using a bi-exponential function with the function parameters serving as state variables. A linear function is fitted to the HF as the measured quantity. The estimation results are depicted in Fig. 17(d)-(e), 18(d)-(e), and 19. One can see that the estimation of the MCCEKF is still notable due to the robustness of the MCC, displaying resistance against outlier disturbances. However, it should be recognized that there is no fixed expression for the physical equations governing SOH. Furthermore, all the fitted parameters are only relevant to the specific cell being analyzed. Consequently, the estimation of SOH requires the parameters to be specifically adjusted for each individual cell, resulting in a paradoxical situation. This predicament is one of the contributing factors contributing to the complexities associated with applying MD methods.

In addition, the GELMs of Sections V.B and V.C both show good estimation results under different datasets and the same parameters, responding to the more stable performance of the GELM than the ELM.

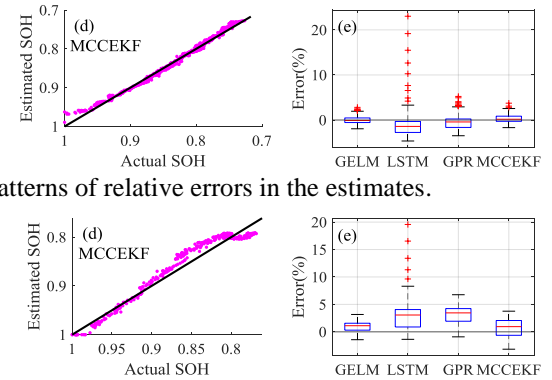


Fig. 19. Comparison of model RMSE (%) and MAPE (%). (a) Battery1. (b) Battery3.

GELM. The strength of the proposed framework lies in its ability to suppress unknown distributional noise in the measurement data, especially the non-Gaussian noise in it, which is attributed to the good performance of GCL. Another advantage is the simplicity of the framework's structure, thanks to the SG-GCL, which is based on polynomial fitting only, and GELM, a neural network with only one hidden layer, so that the computational complexity of the framework is mainly affected by the amount of data and less by its own structure.

However, the proposed framework still has some technical challenges listed as

- 1) Hyperparameter tuning within the proposed framework presents a challenge. While leveraging the strong performance of GCL and human expertise allows for the relatively easy identification of satisfactory parameters, achieving globally optimal parameters proves more difficult. This necessitates the exploration of alternative approaches to determine optimal parameters. Since the individual hyperparameters also interact with each other, optimization can only be performed for all used hyperparameters together. Iterative optimization of the hyperparameters can be carried out in the feasible domain,

> REPLACE THIS LINE WITH YOUR MANUSCRIPT ID NUMBER (DOUBLE-CLICK HERE TO EDIT) <

e.g., by bionic optimization algorithms or grid search algorithms. Or it can be attempted using novel methods such as transfer learning and reinforcement learning.

2) Computational overhead (CO). Since the CO of the SG-GCL filter considering the fixed-point iteration is highly influenced by the amount of data, several faster optimization algorithms (e.g. quasi-newton method and adaptive iteration strategies) or approximation and reduced precision techniques (including approximate GCL and lower-precision fixed-pint) may be utilized to address the CO issue to meet the demands of practical applications, which will be a major research direction for in-depth investigation in our future work.

3) Validation in practical applications. As an initial stemming from Contribution 2 of this article, the limited volume of SOH data restricts current validation to the dataset collected within our laboratory. Furthermore, recognizing that the aging patterns of LIB are influenced by user behavior and various unforeseen factors, and thus the applicability of the proposed framework under more complex conditions warrants further investigation. Specifically, we will continue to collect data under different operating conditions in our labs to achieve data that is more in line with users' real-world usage habits and to expand the data set. In addition, we are looking forward to working with manufacturers of electric vehicles etc. to validate the framework under real data.

The above challenges are exactly the direction of our next research and the problems that need to be solved.

VII. CONCLUSION

Measurement noise or outliers may be introduced during LIB data acquisition, which can affect the state estimation results of the BMS. In this article, a filter is combined with a data-driven approach to address the challenge of unknown distribution noise in the measurement data and labelled values. The SG-GCL filter with GCL is developed to filter out the noise from the measurement data. Compared to the HF extracted from unfiltered data, the Pearson correlation between the filtered extracted HF and SOH is improved by 0.4963, which demonstrates that this measure greatly improves the validity of the extracted HF. Meanwhile, this result leads to a 43.69% reduction in the RMSE metric of the ELM estimation of SOH, which indicates that the data filtering process also contributes to the improvement of the accuracy of the SOH estimation. For the noise in the training labelled values, an ELM model with GCL based estimation model is introduced in this study. The validation results on laboratory data and public datasets show that it can alleviate the influence of noise in the labelled values on the model training process to a certain extent, which in turn improves the SOH estimation accuracy. Employing the proposed GELM model yields a notable reduction in RMSE of 0.66% compared to the standard ELM. In addition, the GELM also demonstrates significant advantages over several existing classical methods. In all, the proposed SOH estimation framework since the combination of SG-GCL and GELM in this article can performs a stable and effective performance.

REFERENCES

- [1] X. Gong, R. Xiong, and C. C. Mi, "Study of the Characteristics of Battery Packs in Electric Vehicles With Parallel-Connected Lithium-Ion Battery Cells," *IEEE Transactions on Industry Applications*, vol. 51, no. 2, pp. 1872–1879, Mar. 2015.
- [2] Z. Zhao, H. Hu, Z. He, H. Ho, P. Davari, and F. Blaabjerg, "Power Electronics-Based Safety Enhancement Technologies for Lithium-Ion Batteries: An Overview From Battery Management Perspective," *IEEE Transactions on Power Electronics*, vol. 38, no. 7, pp. 8922–8955, Jul. 2023.
- [3] X. Bian, Z. Wei, W. Li, J. Pou, D. U. Sauer, and L. Liu, "State-of-Health Estimation of Lithium-ion Batteries by Fusing an Open-Circuit-Voltage Model and Incremental Capacity Analysis," *IEEE Transactions on Power Electronics*, vol. 37, no. 2, pp. 2226–2236, Jan. 2021.
- [4] S. Bamati and H. Chaoui, "Developing an Online Data-Driven State of Health Estimation of Lithium-ion Batteries under Random Sensor Measurement Unavailability," *IEEE Transactions on Transportation Electrification*, vol. 9, no. 1, pp. 1128–1141, 2022.
- [5] X. Shu, J. Shen, G. Li, Y. Zhang, Z. Chen, and Y. Liu, "A Flexible State-of-Health Prediction Scheme for Lithium-Ion Battery Packs With Long Short-Term Memory Network and Transfer Learning," *IEEE Transactions on Transportation Electrification*, vol. 7, no. 4, pp. 2238–2248, Dec. 2021.
- [6] Z. Wei, H. Ruan, Y. Li, J. Li, C. Zhang, and H. He, "Multi-Stage State of Health Estimation of Lithium-ion Battery with High Tolerance to Heavily-Partial Charging," *IEEE Transactions on Power Electronics*, vol. 37, no. 6, pp. 7432–7442, 2022.
- [7] Y. Li, M. Maleki, and S. Banitaan, "State of health estimation of lithium-ion batteries using EIS measurement and transfer learning," *Journal of Energy Storage*, vol. 73, Dec. 2023, Art. no. 100951.
- [8] B. Gou, Y. Xu, and X. Feng, "An Ensemble Learning-Based Data-Driven Method for Online State-of-Health Estimation of Lithium-Ion Batteries," *IEEE Transactions on Transportation Electrification*, vol. 7, no. 2, pp. 422–436, Jun. 2021.
- [9] J. Wu, H. Su, J. Meng, and M. Lin, "State of Health Estimation for Lithium-Ion Battery via Recursive Feature Elimination on Partial Charging Curves," *IEEE Journal of Emerging and Selected Topics in Power Electronics*, vol. 11, no. 1, pp. 131–142, Jan. 2022.
- [10] L. Cai, J. Meng, D. I. Stroe, J. Peng, G. Luo, and R. Teodorescu, "Multiobjective Optimization of Data-Driven Model for Lithium-Ion Battery SOH Estimation With Short-Term Feature," *IEEE Transactions on Power Electronics*, vol. 35, no. 11, pp. 11855–11864, Nov. 2020.
- [11] L. Cai and J. Lin, "A charging-feature-based estimation model for state of health of lithium-ion batteries," *Expert Systems with Applications*, vol. 238, Mar. 2024, Art. no. 122034.
- [12] L. Zhou, Y. Zhao, D. Li, and Z. Wang, "State-of-Health Estimation for LiFePO₄ Battery System on Real-World Electric Vehicles Considering Aging Stage," *IEEE Transactions on Transportation Electrification*, vol. 8, no. 2, pp. 1724–1733, Jun. 2022.
- [13] E. Kheirkhah-Rad, A. Parvareh, M. Moeini - Aghtaei, and P. Dehghanian, "A Data-Driven State-of-Health Estimation Model for Lithium-Ion Batteries Using Referenced-Based Charging Time," *IEEE Transactions on Power Delivery*, vol. 38, no. 5, pp. 3406–3416, Oct. 2023.
- [14] Z. Deng, X. Hu, P. Li, X. Lin, and X. Bian, "Data-Driven Battery State of Health Estimation Based on Random Partial Charging Data," *IEEE Transactions on Power Electronics*, vol. 37, no. 5, pp. 5021–5031, May 2022.
- [15] J. He, Z. Wei, X. Bian, and F. Yan, "State-of-Health Estimation of Lithium-Ion Batteries Using Incremental Capacity Analysis Based on Voltage-Capacity Model," *IEEE Transactions on Transportation Electrification*, vol. 6, no. 2, pp. 417–426, Jun. 2020.
- [16] Z. Zhou, B. Duan, Y. Kang, Y. Shang, and Q. Zhang, "Practical State of Health Estimation for LiFePO₄ Batteries Based on Gaussian Mixture Regression and Incremental Capacity Analysis," *IEEE Transactions on Industrial Electronics*, vol. 70, no. 3, pp. 2576–2585, Mar. 2023.
- [17] L. Mao, H. Hu, J. Chen, J. Zhao, K. Qu, and L. Jiang, "Online State of Health Estimation Method for Lithium-ion Battery Based on

> REPLACE THIS LINE WITH YOUR MANUSCRIPT ID NUMBER (DOUBLE-CLICK HERE TO EDIT) <

- CEEMDAN for Feature Analysis and RBF Neural Network," *IEEE Journal of Emerging and Selected Topics in Power Electronics*, vol. 11, no. 1, pp. 187–200, 2021.
- [18] H. Zhao, Z. Chen, X. Shu, J. Shen, Z. Lei, and Y. Zhang, "State of health estimation for lithium-ion batteries based on hybrid attention and deep learning," *Reliability Engineering & System Safety*, vol. 232, Apr. 2023, Art. no. 109066.
- [19] H. Xu, L. Wu, S. Xiong, W. Li, A. Garg, and L. Gao, "An improved CNN-LSTM model-based state-of-health estimation approach for lithium-ion batteries," *Energy*, vol. 276, Aug. 2023, Art. no. 127585.
- [20] L. Li, Y. Li, W. Cui, Z. Chen, et al., "A novel health indicator for online health estimation of lithium-ion batteries using partial incremental capacity and dynamic voltage warping," *Journal of Power Sources*, vol. 545, Oct. 2022, Art. no. 231961.
- [21] L. Zhang, W. Wang, H. Yu, Z. Zhang, et al., "Remaining useful life and state of health prediction for lithium batteries based on differential thermal voltammetry and a deep learning model," *iScience*, vol. 25, no. 12, Nov. 2022.
- [22] F. Guo, X. Wu, L. Liu, J. Ye, et al., "Prediction of remaining useful life and state of health of lithium batteries based on time series feature and Savitzky-Golay filter combined with gated recurrent unit neural network," *Energy*, vol. 270, May 2023, Art. no. 126880.
- [23] M. Sadeghi, F. Behnia, and R. Amiri, "Window Selection of the Savitzky-Golay Filters for Signal Recovery from Noisy Measurements," *IEEE Transactions on Instrumentation and Measurement*, vol. 69, no. 8, pp. 5418–5427, Aug. 2020.
- [24] C. She, Y. Li, Y. Wang, T. Wik, Z. Wang, and F. Sun, "Offline and Online Blended Machine Learning for Lithium-Ion Battery Health State Estimation," *IEEE Transactions on Transportation Electrification*, vol. 8, no. 2, pp. 1604–1618, Nov. 2021.
- [25] J.-S. Hong, Y. Chen, Q. Chai, Q. Lin, and W. Wu, "State-of-health estimation of lithium-ion batteries using a novel dual-stage attention mechanism based recurrent neural network," *Journal of Energy Storage*, vol. 72, Nov. 2023, Art. no. 109297.
- [26] Q. Wang, Z. Wang, L. Zhang, P. Liu, and L. Zhou, "A Battery Capacity Estimation Framework Combining Hybrid Deep Neural Network and Regional Capacity Calculation Based on Real-World Operating Data," *IEEE Transactions on Industrial Electronics*, vol. 70, no. 8, pp. 8499–8508, Aug. 2023.
- [27] Y. Zhou, G. Dong, Q. Tan, X. Han, C. Chen, and J. Wei, "State of health estimation for lithium-ion batteries using geometric impedance spectrum features and recurrent Gaussian process regression," *Energy*, vol. 262, Jan. 2023, Art. no. 125514.
- [28] Z. Pang, K. Yang, Z. Song, P. Niu, G. Chen, and J. Meng, "A new method for determining SOH of lithium batteries using the real-part ratio of EIS specific frequency impedance," *Journal of Energy Storage*, vol. 72, Nov. 2023, Art. no. 108693.
- [29] Y. Fu, J. Xu, M. Shi, and X. Mei, "A Fast Impedance Calculation-Based Battery State-of-Health Estimation Method," *IEEE Transactions on Industrial Electronics*, vol. 69, no. 7, pp. 7019–7028, Jul. 2022.
- [30] J. Wu, X. Cui, H. Zhang, and M. Lin, "Health Prognosis With Optimized Feature Selection for Lithium-Ion Battery in Electric Vehicle Applications," *IEEE Transactions on Power Electronics*, vol. 36, no. 11, pp. 12646–12655, Apr. 2021.
- [31] B. Chen, L. Xing, H. Zhao, N. Zheng, and J. C. Principe, "Generalized Correntropy for Robust Adaptive Filtering," *IEEE Transactions on Signal Processing*, vol. 64, no. 13, pp. 3376–3387, Jul. 2016.
- [32] W. Liu, P. P. Pokharel, and J. C. Principe, "Correntropy: Properties and Applications in Non-Gaussian Signal Processing," *IEEE Transactions on Signal Processing*, vol. 55, no. 11, pp. 5286–5298, Nov. 2007.
- [33] Z. Li, W. Chen, Y. Sun, and Z. Chen, "An Improved Multiple-Outlier Robust Filter Based on Maximum Correntropy Criterion for Integrated Navigation," *IEEE Sensors Journal*, vol. 23, no. 15, pp. 17451–17461, Aug. 2023.
- [34] B. Du, X. Tang, Z. Wang, L. Zhang, and D. Tao, "Robust Graph-Based Semisupervised Learning for Noisy Labeled Data via Maximum Correntropy Criterion," *IEEE Transactions on Cybernetics*, vol. 49, no. 4, pp. 1440–1453, Apr. 2019.
- [35] Y. Wang, Z. Yang, Y. Wang, Z. Li, V. Dinavahi, and J. Liang, "Resilient Dynamic State Estimation for Power System Using Cauchy-Kernel-Based Maximum Correntropy Cubature Kalman Filter," *IEEE Transactions on Instrumentation and Measurement*, vol. 72, Jan. 2023, Art. no. 3268445.
- [36] B. Chen, X. Wang, N. Lu, S. Wang, J. Cao, and J. Qin, "Mixture correntropy for robust learning," *Pattern Recognition*, vol. 79, pp. 318–327, Jul. 2018.
- [37] W. He, N. Williard, M. Osterman, and M. Pecht, "Prognostics of lithium-ion batteries based on Dempster-Shafer theory and the Bayesian Monte Carlo method," *Journal of Power Sources*, vol. 196, no. 23, pp. 10314–10321, Dec. 2011.
- [38] "Panasonic Industry Co., Ltd." [Online]. Available: <https://industrial.panasonic.cn/index.php/ww/products>.
- [39] H. Chen, E. Tian, L. Wang, and S. Liu, "A Joint Online Strategy of Measurement Outliers Diagnosis and State of Charge Estimation for Lithium-Ion Batteries," *IEEE Transactions on Industrial Informatics*, vol. 19, no. 5, pp. 6387–6397, May 2023.
- [40] G. Ma, S. Xu, T. Yang, et al., "A Transfer Learning-Based Method for Personalized State of Health Estimation of Lithium-Ion Batteries," *IEEE transactions on neural networks and learning systems*, vol. 35, no. 1, pp. 759–769, Jan. 2022.
- [41] X. Hu, Y. Che, X. Lin, and S. Onori, "Battery Health Prediction Using Fusion-Based Feature Selection and Machine Learning," *IEEE Transactions on Transportation Electrification*, vol. 7, no. 2, pp. 382–398, Jun. 2021.
- [42] Z. Shi, J. Xiao, J. Jiang, Y. Zhang, and Y. Zhou, "Identifying Reliability High-Correlated Gates of Logic Circuits With Pearson Correlation Coefficient," *IEEE Transactions on Circuits & Systems II Express Briefs*, vol. 71, no. 4, pp. 2319–2323, Jan. 2024.
- [43] D. Liu, X. Yin, Y. Song, W. Liu, and Y. Peng, "An On-Line State of Health Estimation of Lithium-Ion Battery Using Unscented Particle Filter," *IEEE Access*, vol. 6, pp. 40990–41001, 2018.